Theory and Modeling of ULF Waves

Robert L. Lysak (U. Minnesota)
Collaborators: Yan Song (U. Minn.), Colin L. Waters, Murray D. Sciffer (U.Newcastle)

- ULF waves are important for transferring energy throughout the magnetosphere and, in particular, carrying changes in the field-aligned current

- These waves can be modeled by global MHD simulations
  - However, only longer period ULF waves can be accurately modeled.
  - In addition, near-Earth region “gap” not modeled.

- Propagation of Alfvén waves strongly affected by plasma inhomogeneity and coupling to the ionosphere.

- Linearized wave models can give a good description of magnetosphere-ionosphere coupling by Alfvén waves

Outline

- Introduction to ULF waves
  - Dispersion relations and terminology
  - Field line resonances and phase mixing
  - Interaction with the ionosphere
- Global MHD Models
  - Response to dayside transients
  - Response to fast flows in the tail
- Linearized Wave Models
  - Pi2 propagation
  - Internal sources: Poloidal Pc4
  - Pi1/Pc1 waves: higher frequencies require height-resolved ionosphere

MHD Wave Modes

- Linearized MHD equations give 3 wave modes:
  - Slow mode (ion acoustic wave): $\omega = k_{\parallel} c_s \quad \left(c_s = \sqrt{\gamma p / \rho}\right)$
    - Plasma and magnetic pressure balance along magnetic field
    - Electron pressure coupled to ion inertia by electric field
  - Intermediate mode (shear Alfvén wave): $\omega = k_{\parallel} V_A \quad \left(V_A = B / \sqrt{\mu_0 \rho}\right)$
    - Magnetic tension balanced by ion inertia
    - Guided along geomagnetic field
    - Carries field-aligned current
  - Fast mode (magnetosonic wave): $\omega = \sqrt{k^2 V_A^2 + k_{\perp}^2 c_s^2}$
    - Magnetic and plasma pressure balanced by ion inertia
    - Transmits total pressure variations across magnetic field
- These dispersion relations are valid for a uniform plasma: modes can be coupled by inhomogeneity

(Note dispersion relations given are in low β limit)

Magnetospheric ULF Waves: Terminology

- MHD waves with periods from 0.2 – 600 sec (1.7 mHz – 5 Hz) are classified as “Pc” (continuous) or “Pi” (irregular) with number giving frequency range:
  - Pc1 (0.2-5 s), Pc2 (5-10 s), Pc3 (10-45 s), Pc4 (45-150 s) and Pc5 (150-600 s)
  - Pi1 (1-40 s), Pi2 (40-150 s)
- Dipole field parameterized by L (equatorial distance in Earth radii)
- Dipole coordinates: ν (=1/L, outward or poleward); φ (azimuthal, usually measured in Magnetic Local Time, MLT); μ (field-aligned)
- Azimuthal mode number *m* often used ($e^{im\varphi}$ dependence)
- Waves classified as *toroidal* (E_ν, B_φ) or *poloidal* (E_φ, B_ν)
- At low *m*, poloidal mode is compressional (fast mode) while toroidal is guided along field (shear Alfvén mode)
- At high *m*, toroidal mode is compressional and poloidal is guided.

Density and Alfvén speed profiles

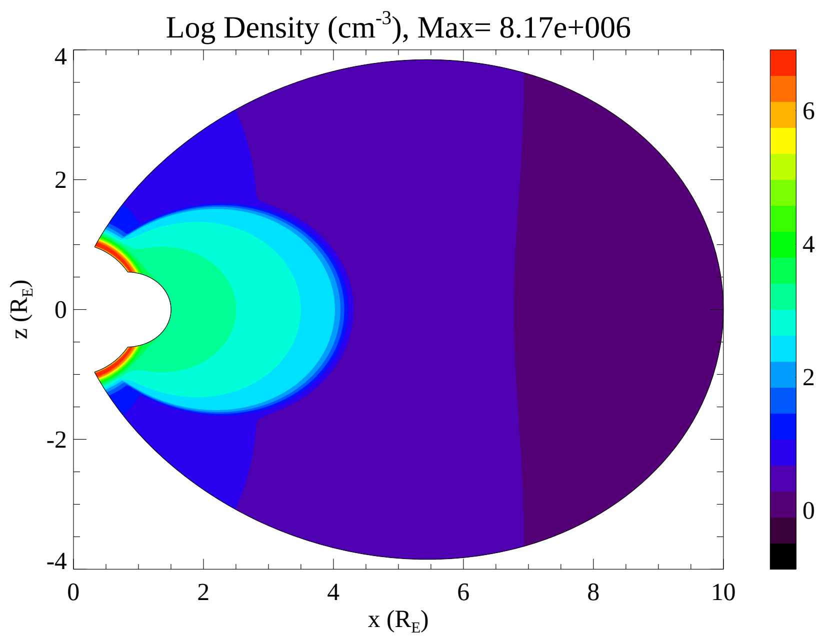

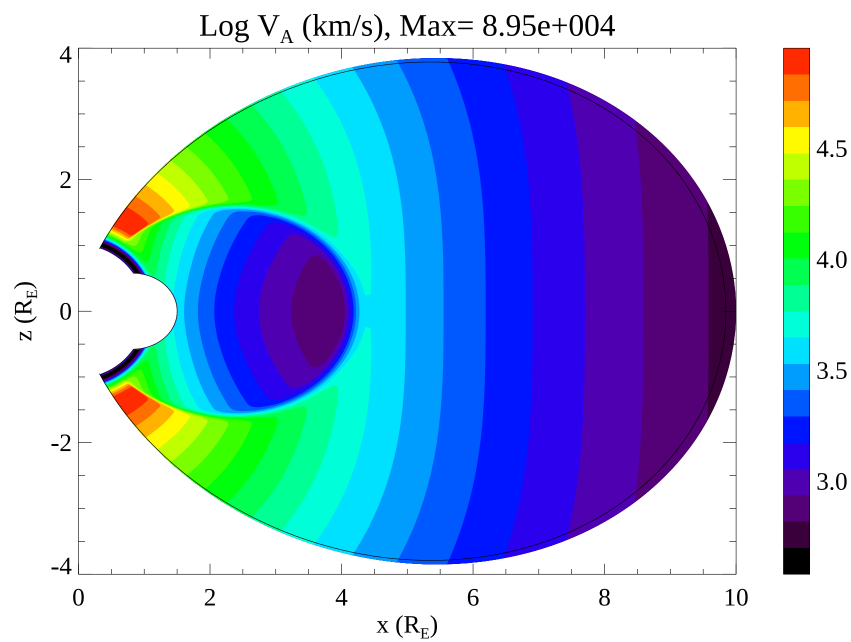

- Model based on ionospheric model as in Kelley (1989), plasmasphere model of Chappell (1972), $1/r$ density dependence along high-latitude field lines.
- Plasmapause at L=4, width of transition 0.1 R_E

Alfvén Waves are like waves on a string: Field Line Resonances

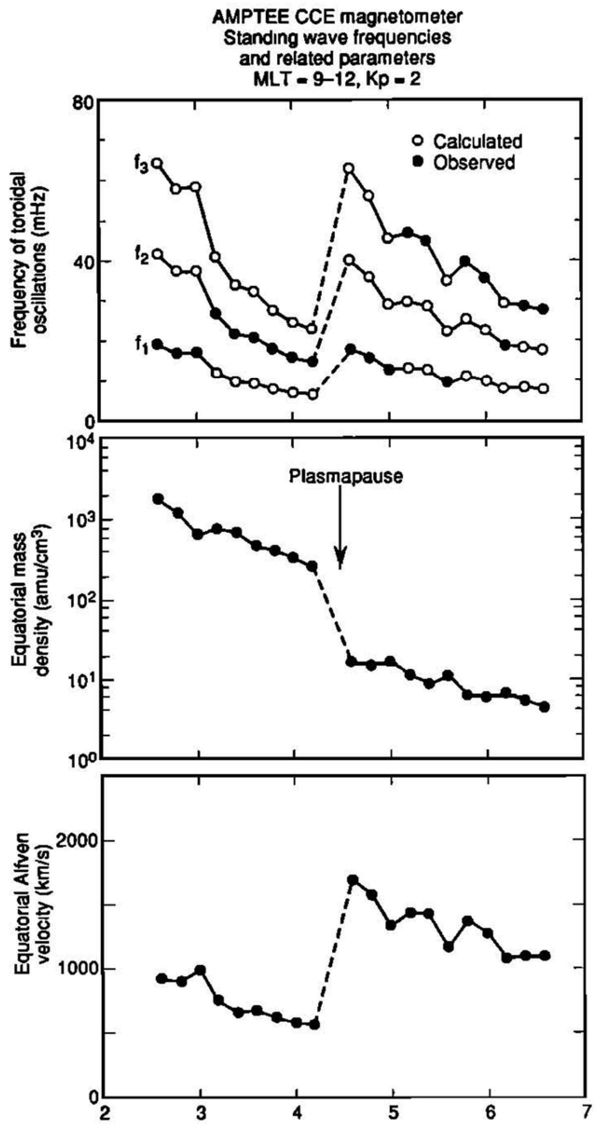

Takahashi and Anderson, 1992

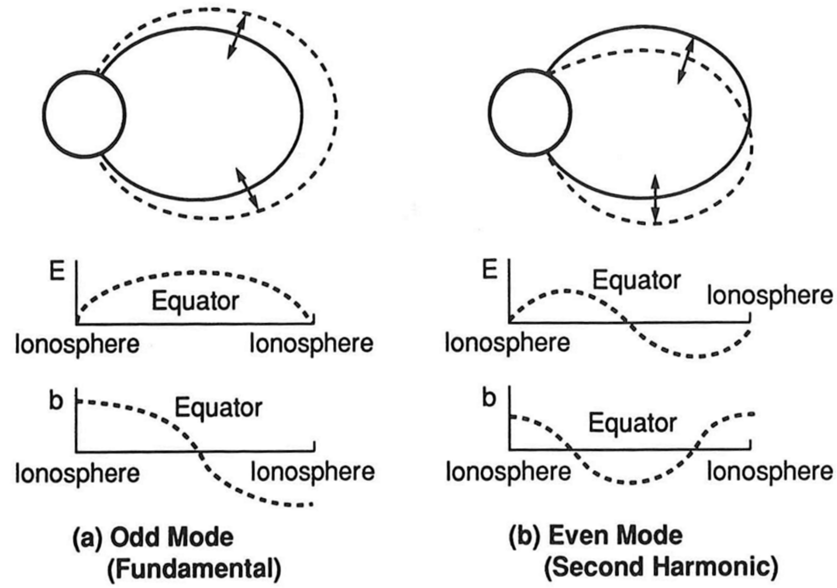

Kivelson and Russell, 1995

Above: Harmonic structure of FLR. Note that highly conductive ionosphere leads to node in electric field.

Left: Observations of Field Line Resonance frequencies. Top panel gives first 3 harmonic frequencies, middle gives inferred density profile and bottom is inferred Alfvén speed: frequencies ~ 10-20 mHz (50-100 sec period)

•

Excitation of Field Line Resonances: Linear mode conversion

- Low-*m* compressional waves can be excited by compression at the magnetopause or the plasma sheet
  - Dynamic pressure fluctuations in solar wind
  - Kelvin-Helmholtz instability
  - Fast flows from magnetotail; dipolarization fronts
- For azimuthal symmetry (m=0) compressional and shear Alfvén modes uncoupled
  - Compressional mode gives “breathing” mode: radial velocities
  - Shear Alfvén waves carry field-aligned current
- Finite values of *m* lead to mode coupling between shear and compressional waves
- High-*m* waves are shielded from the inner magnetosphere; such waves are generated internally by plasma instabilities, e.g., drift-bounce resonance

Fast mode cutoff at large m

- Fast mode propagates isotropically, $\omega = kV_A$
- Total k must be bigger than azimuthal component, $k_\varphi = m/r \sin\theta$
- At a given frequency f (in Hz), fast mode waves cannot propagate if $m > 2\pi fr \sin\theta/V_A$, plotted below for $f = 20$ mHz

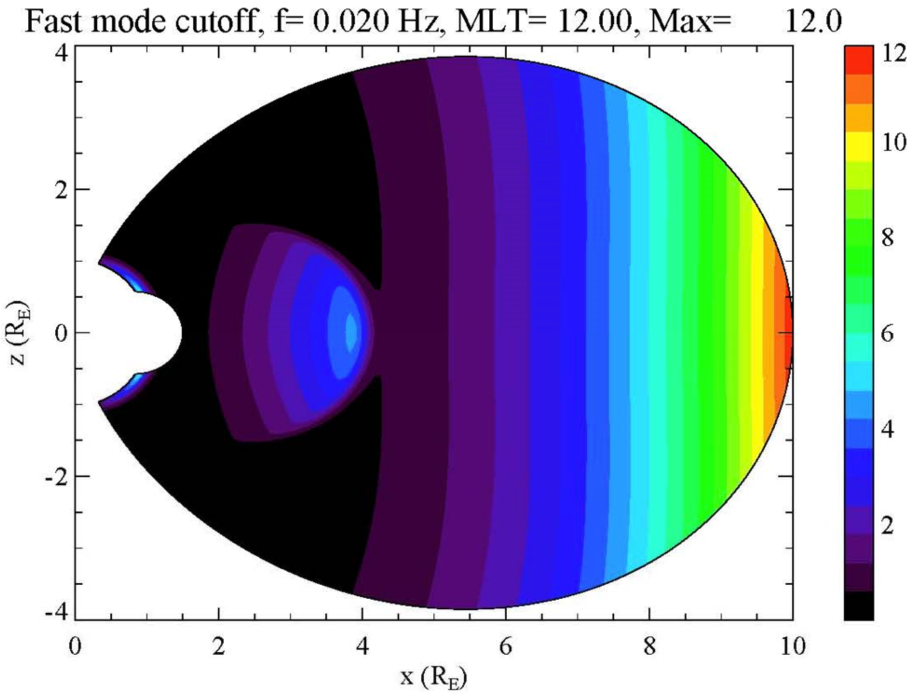

Production of Small Scales: Phase Mixing

- Gradients in the Alfvén speed lead to phase mixing, producing smaller perpendicular scales (basic mechanism behind field line resonance.)

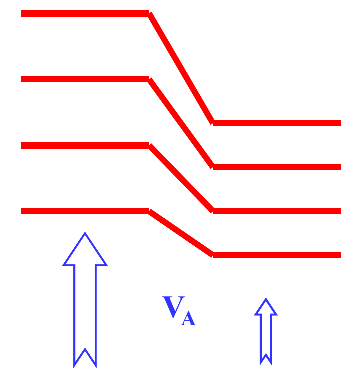

- Such gradients are always present, especially in boundary regions:
  - Plasma Sheet Boundary Layer: poleward boundary of aurora
  - Boundaries of aurora density cavities (e.g., Chaston et al., 2006, at right)

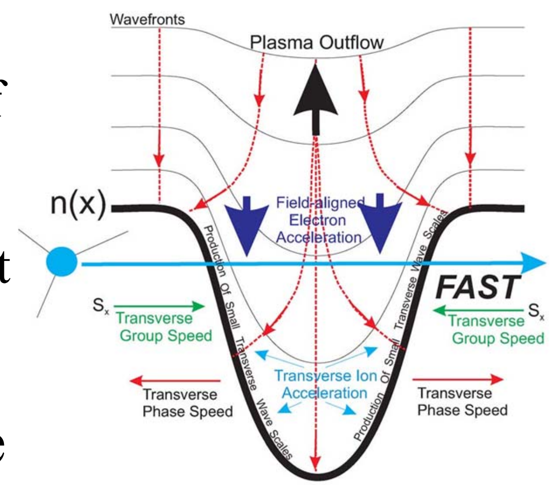

- Scale length estimated to be ~ $(\Sigma_A/\Sigma_P)\, L_0$, where $\Sigma_A = 1/\mu_0 V_A$ is Alfvén conductance and L_0 is gradient scale length.

Reflection of Alfvén Waves by the Ionosphere

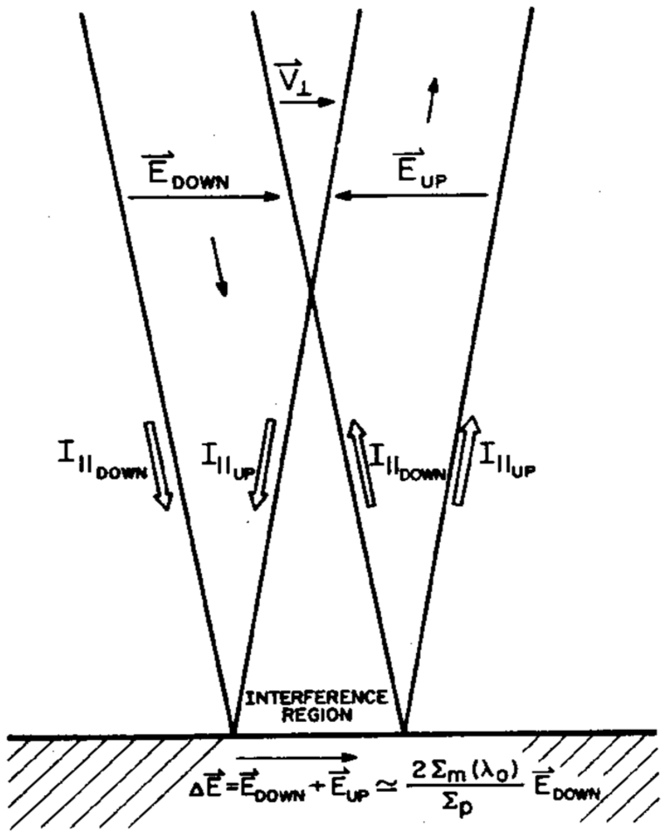

(Mallinckrodt and Carlson, 1978)

- Ionosphere acts as terminator for Alfvén transmission line, with admittance $\Sigma_A = 1/\mu_0 V_A$.
- But, impedances don't match: wave is reflected
- Usually $\Sigma_P >> \Sigma_A$, so electric field of reflected wave is reversed ("short-circuit")
- Reflection coefficient:

$$R = \frac{E_{up}}{E_{down}} = \frac{\Sigma_A - \Sigma_{P,eff}}{\Sigma_A + \Sigma_{P,eff}}$$

- Effective Pedersen conductivity modified by Hall conductance, parallel electric fields

Modeling ULF waves with Global MHD

- A number of authors have used global MHD to model ULF waves (Claudepierre et al., 2010, 2016; Ream et al, 2013, 2015; Shi et al., 2013)
- Advantages of this approach:
  - Fully nonlinear MHD; Self-consistent magnetic geometry
  - Direct driving by solar wind fluctuations
  - Open system: waves can propagate out of tail
- System can be driven by idealized solar wind conditions (to understand system response) or by conditions observed by upstream monitors (to simulate actual events)

Driving with sinusoidal dynamic pressure

- Claudepierre et al. (2010) drove LFM model with sinusoidal dynamic pressure variations, 10 mHz case shown
- Field line resonance appears at L ~ 7 (white field line)
- Pressure perturbation drives strongest waves off the Sun-Earth line (9, 15 MLT)
- Spectrum (d) and mode structure (e) show fundamental field line resonance
  - Apparent nodes in E_r since cylindrical coordinates used; E_r is parallel to B_0 at two points

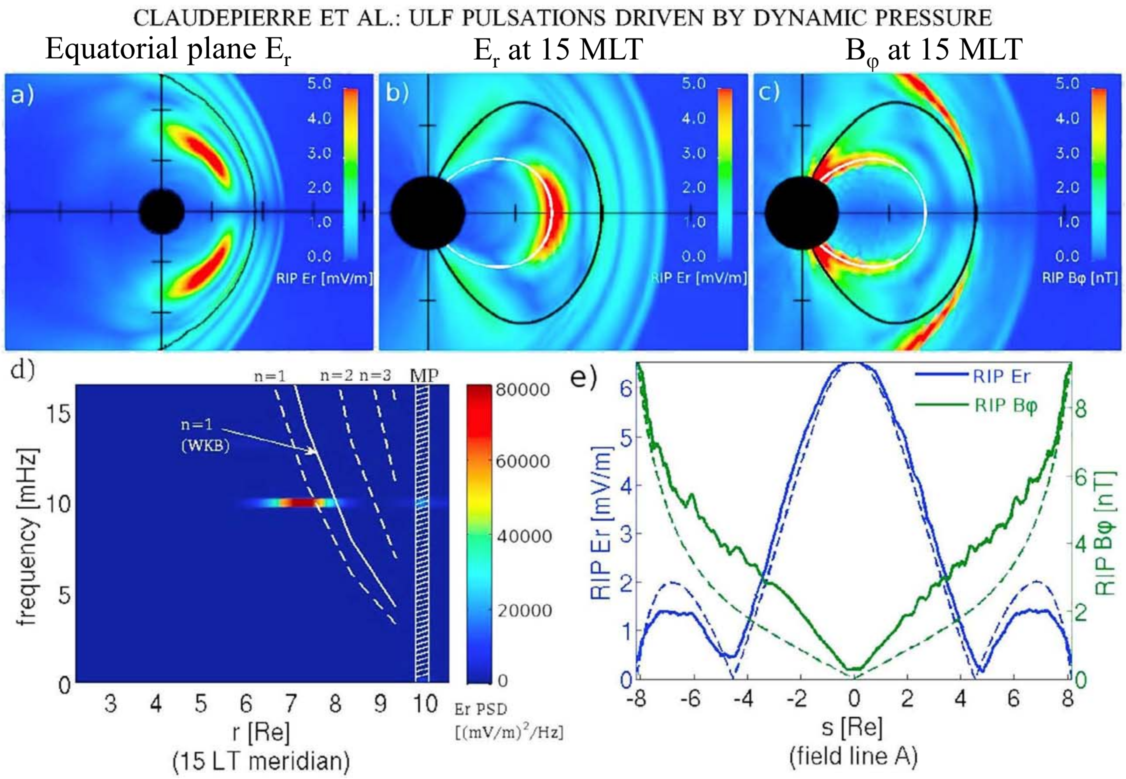

E_r: blue
B_φ: green
Solid: simulation
Dashed: Dipole solution

Response to a sudden impulse

- Shi et al. (2013, 2014) studied SI events from THEMIS, coupled with OpenGGCM simulations (Raeder et al., 2008)
- Of 13 events studied, 3 showed evidence of field line resonances (missed in other cases?)
- Simulations are suggestive of vortex structure near magnetopause caused by pressure imbalance as fast mode wave propagates faster than solar wind to tail (Sibeck, 1990)
- Vortex structure can mode convert to shear Alfvén wave at field line resonances

SHI ET AL.: SI-INDUCED ULF WAVE IN THE NIGHTSIDE PLASMA SHEET

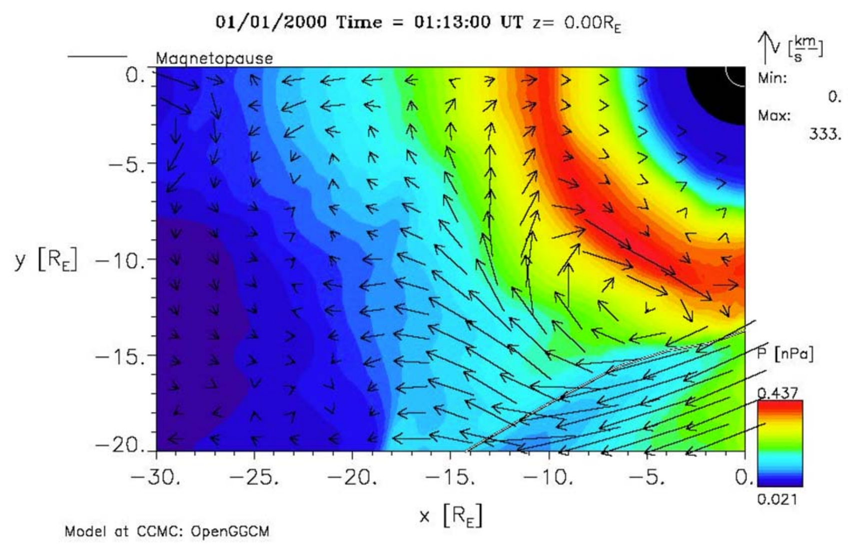

Bursty flows and Pi2 pulsations

- Substorms are associated with bursty bulk flows (BBFs) that can lead to oscillations in the Pi2 range
- Global MHD models (Ream et al., 2013, 2015; Fujita and Tanaka, 2013) have been used to model this interaction
- Leading edge of BBF is referred to as dipolarization front, which often has slow mode character, but can launch a fast mode wave (Kepko et al., 2001) that runs ahead of the flow
- Sides of BBF show strong vorticity in the flow, providing a direct means for field-aligned current generation
- Braking of BBF can be oscillatory due to overshoot and rebound, possibly providing a source (Panov et al., 2013, 2014)
- At low latitudes, plasmaspheric virtual resonance can trap waves at Pi2 frequencies (Lee and Kim, 1999)

Comparison of Two Global MHD Models

- Ream et al. (2015) used UCLA model (Raeder et al., 1998; El-Alaoui, 2001) and LFM model (Lyon et al., 2004)
- Results are shown in terms of radial-distance vs. time plots below
- Note these models have no plasmasphere, so no plasmaspheric resonance

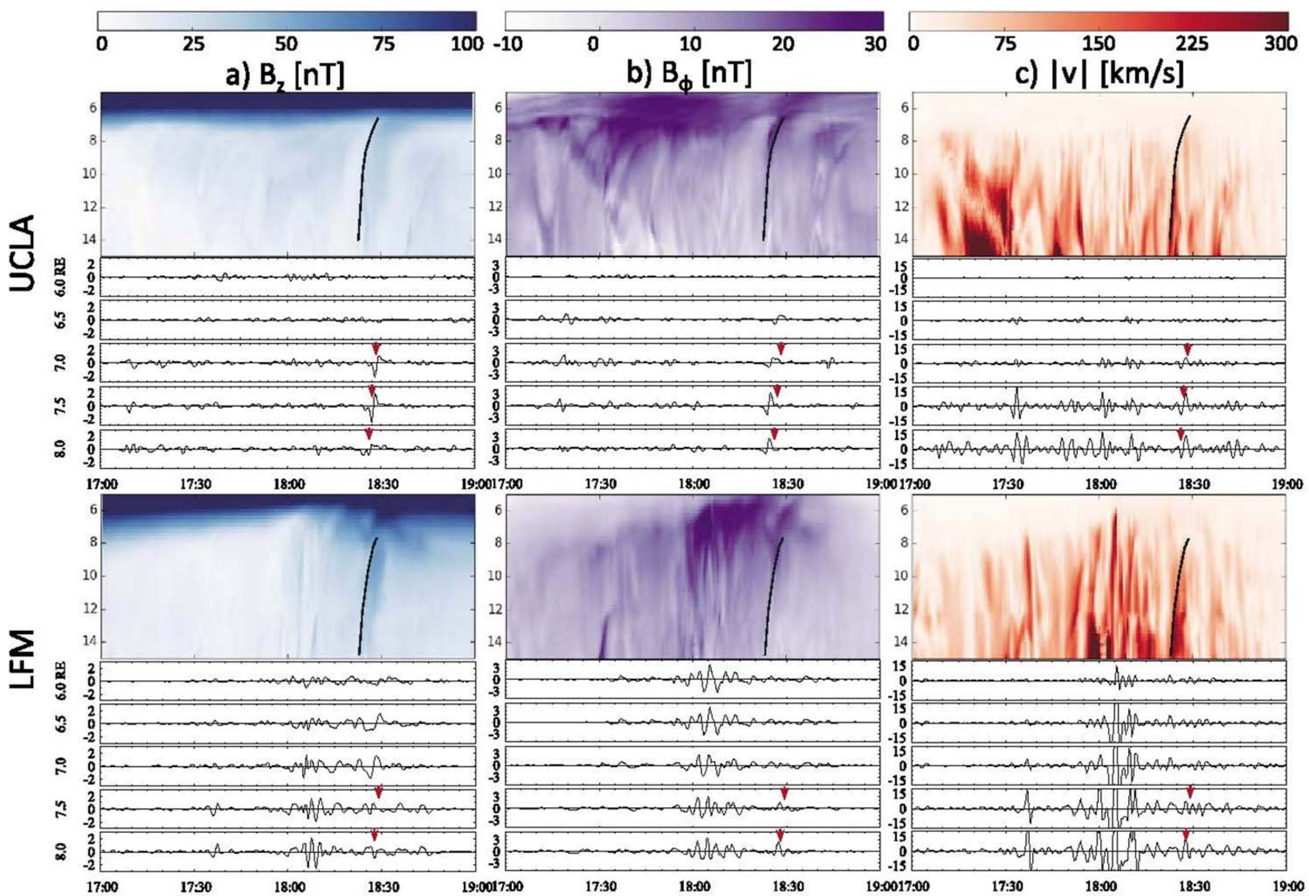

Effect of the plasmasphere

- Claudepierre et al. (2016) have recently done first global MHD simulations with a plasmasphere, based on the coupled LFM/RCM model
- Dense plasmasphere lowers the Alfvén speed, producing peak in Alfvén speed just outside the plasmapause
- Radial electric field shows toroidal field line resonance, azimuthal E and parallel B give compressional mode (dotted lines are plasmapause and magnetopause

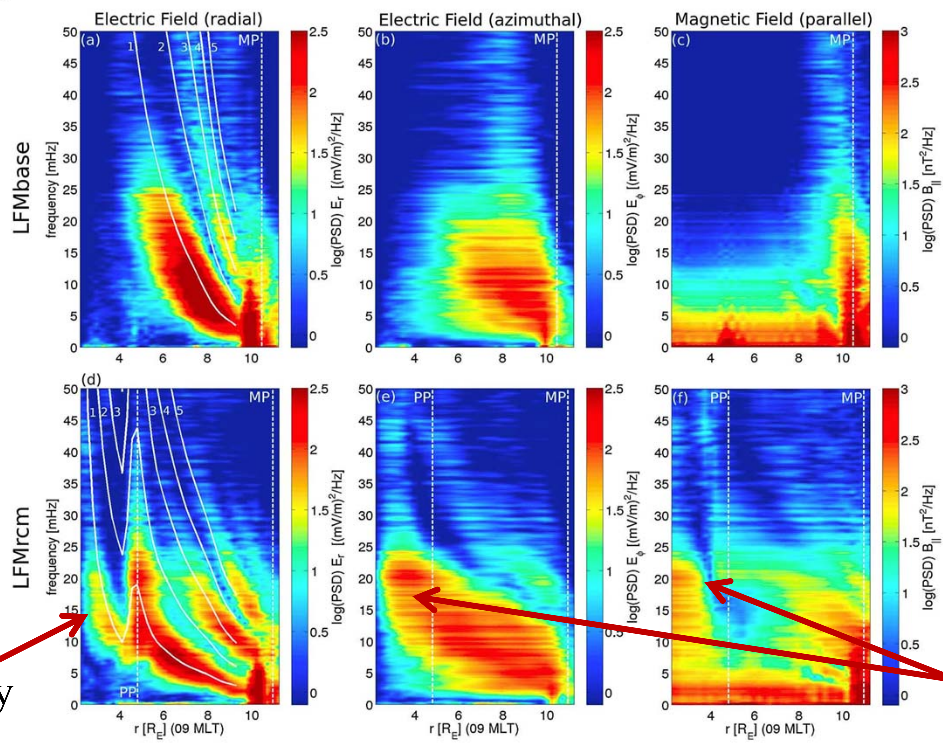

No plasmasphere

With plasmasphere

Reduced FLR frequency

Compressional resonance in plasmasphere

Courant Condition

- A fundamental stability condition is the Courant condition, $\delta t < \delta x/V$, where V is a characteristic speed (wave speed, convection speed, etc.)
  - In other words, information can not move more than the spatial step size in one time step
  - Thus, improving spatial resolution requires smaller time steps
  - Also, higher spatial resolution needed where wave speeds are high
  - In global MHD models, limited spatial resolution implies higher frequency waves are attenuated
    - Example at right (Claudepierre et al., 2010): Blue spectrum is at upstream boundary, green spectrum 10 R_E closer to Earth
  - Near Earth, the Alfvén speed is high and spatial gradients are large, so most global MHD models have inner boundary at 2-3 R_E: “Gap” region

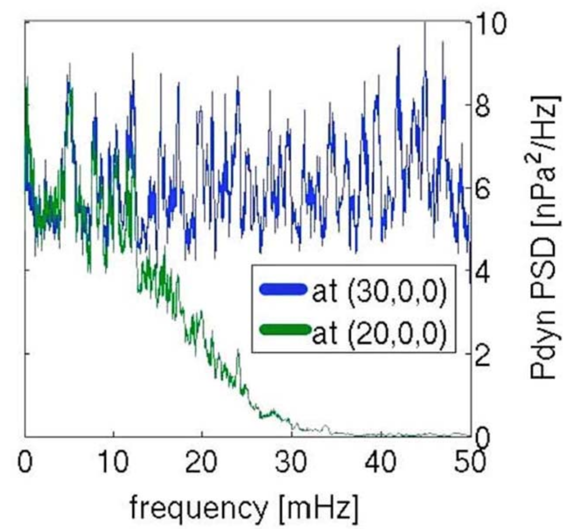

Modeling the "Gap"

- To describe propagation across the high-Alfvén speed gap region, most global MHD codes use an instantaneous mapping from inner simulation boundary to ionosphere.
  - Not such a bad approximation since wave speeds are very fast in this region anyway

- Inner boundary fields are related by assuming current continuity and electrostatic fields in a height-integrated ionosphere: $j_{\parallel} \sin i = -\nabla \cdot \overleftrightarrow{\Sigma} \cdot \nabla \Phi$

- Conductivity tensor can vary with local time, solar activity, and electron precipitation: various MHD models treat this somewhat differently

- For example, current density can be determined from MHD fields, continuity equation is solved for potential, and the **E**×**B** drift from the resulting electric field is fed back to simulation (in some cases including parallel electric field from Knight relation).

Boris Correction

- Alfvén speed also high in lobes and in inner magnetosphere if plasmasphere is not included
- To limit wave speed, the perpendicular displacement current is included, which modifies wave speed to $c_A = V_A / \sqrt{1 + V_A^2 / c^2}$
- In real world, this keeps the Alfvén speed less than the speed of light
- In simulations, an artificially low speed of light gives lower limit to wave speed, allowing for larger time step: Boris correction (Boris, 1970)
- Often this has no practical effect on simulation, but for ULF wave studies it can lead to incorrect resonant frequencies

Usefulness of linearized models

- As we've seen, global models do not provide a good description close to the Earth, especially in auroral zones where Alfvén speed can approach the (real) speed of light.
- By simplifying the equations by linearization, the Courant condition can be satisfied with smaller time steps without excessive computational time.
- This procedure can also allow for a detailed description of the ionosphere, beyond the usual height-integrated ionosphere assumption.
- These models do not explicitly include solar wind-magnetosphere interaction, but are very useful for numerical experiments that can illustrate the important physical processes.
- Better spatial resolution allows modeling of higher frequency waves (Pc1,2; Pi1)
- The equations can be further simplified by the use of dipolar coordinates.

Orthogonal Dipole Coordinates

- Orthogonal dipolar coordinates have been widely used to model ULF waves in the magnetosphere (e.g,. Radoski, 1967; Lysak, 1985; Lee and Lysak, 1989, 1991; Rankin et al., 1993, 1994; Streltsov and Lotko, 1995, 1999; Fujita et al., 2000, 2001, 2002).
- These are defined by:

$$\nu = -\frac{\sin^2\theta}{r/R_E}\left(= -\frac{1}{L}\right) \qquad \varphi = \varphi \qquad \mu = \frac{\cos\theta}{\left(r/R_E\right)^2}$$

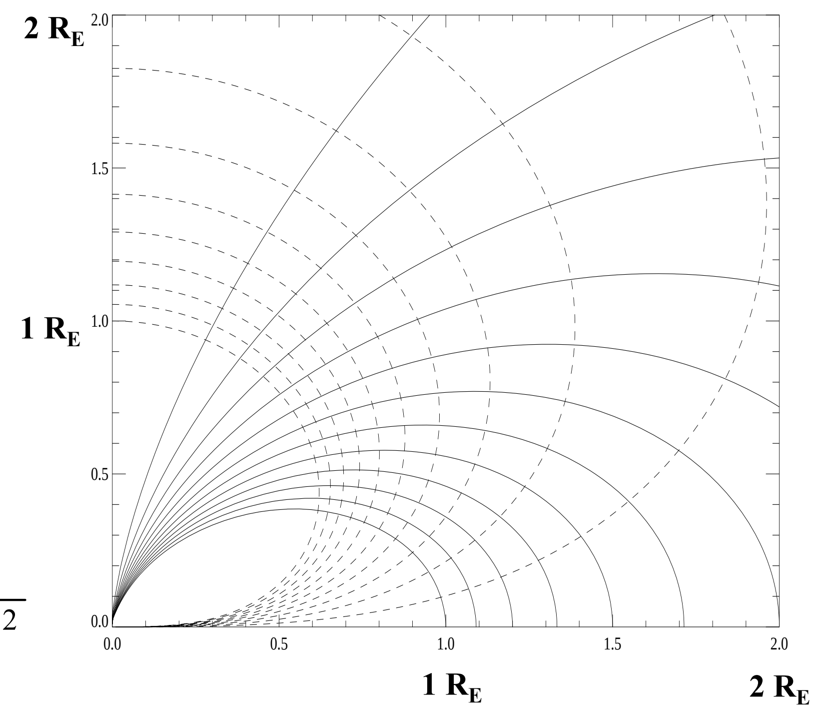

Lines of constant ν (solid) and μ (dashed) within r = 2 R_E

- These give right-handed coordinate system with scale factors

$$h_\nu = \frac{r^2}{R_E \sin\theta\sqrt{1+3\cos^2\theta}} \qquad h_\varphi = r\sin\theta \qquad h_\mu = \frac{r^3}{R_E^2\sqrt{1+3\cos^2\theta}} = \frac{R_E B_0}{B}$$

- Note that the lines of constant μ are close to constant radial distance near pole, but not at lower latitudes.

Wave equations in orthogonal coordinates

- Ideal linear MHD cold plasma equations can be written in terms of Maxwell's equations:

$$\varepsilon_\perp \left(\overleftrightarrow{\mathbf{I}} - \hat{\mathbf{b}}\hat{\mathbf{b}}\right) \cdot \frac{\partial \mathbf{E}}{\partial t} = \frac{1}{\mu_0} \nabla \times \mathbf{B} \qquad \frac{\partial \mathbf{B}}{\partial t} = -\nabla \times \mathbf{E}$$

- Here we have $\varepsilon_\perp = \varepsilon_0(1 + c^2/V_A{}^2)$, and $\hat{\mathbf{b}}$ is the magnetic field direction.

- In orthogonal dipole coordinates, these equations become:

$$\frac{\partial E_\nu}{\partial t} = \frac{V^2}{h_\mu h_\varphi}\left[\frac{\partial}{\partial \varphi}\left(h_\mu B_\mu\right) - \frac{\partial}{\partial \mu}\left(h_\varphi B_\varphi\right)\right]$$

$$\frac{\partial E_\varphi}{\partial t} = \frac{V^2}{h_\nu h_\mu}\left[\frac{\partial}{\partial \mu}\left(h_\nu B_\nu\right) - \frac{\partial}{\partial \nu}\left(h_\mu B_\mu\right)\right]$$

where $V^2 = 1/\varepsilon_\perp \mu_0$ is the Alfven speed

$$\frac{\partial B_\nu}{\partial t} = \frac{1}{h_\mu h_\varphi}\frac{\partial}{\partial \mu}\left(h_\varphi E_\varphi\right)$$

$$\frac{\partial B_\varphi}{\partial t} = -\frac{1}{h_\mu h_\nu}\frac{\partial}{\partial \mu}\left(h_\nu E_\nu\right)$$

$$\frac{\partial B_\mu}{\partial t} = -\frac{1}{h_\nu h_\varphi}\left[\frac{\partial}{\partial \nu}\left(h_\varphi E_\varphi\right) - \frac{\partial}{\partial \varphi}\left(h_\nu E_\nu\right)\right]$$

- Here for azimuthal symmetry, E_ν, B_φ give the shear (toroidal) mode and E_φ, B_ν and B_μ give the compressional (poloidal) mode.

Advantages and Disadvantages of Orthogonal Dipole Coordinates

- These coordinates are easy to define, provide a clear separation of the modes, and distinguish parallel and perpendicular dynamics.
- Mapping factors are built in, e.g., $h_\nu E_\nu$ and $h_\varphi E_\varphi$ are constant along a field line in the electrostatic case.
- Curl equations are easy to implement on a staggered grid.
- However, ionospheric boundary should be at a constant radial distance, rather than constant μ.
- Also, near equator, field lines become very short and coordinate system becomes singular.
- As a result of these conditions and the high Alfvén speed at low altitudes, early models using dipole coordinates did not model the "gap" region

A non-orthogonal dipole coordinate system

- A possible fix is to modify the μ coordinate so that it is constant at the ionospheric distance R_I. Coordinates can now be written in terms of the contravariant coordinates:

$$u^1 = -\frac{R_I \sin^2\theta}{r} \qquad u^2 = \varphi \qquad u^3 = \frac{R_I^2 \cos\theta}{r^2 \cos\theta_I}$$

where θ_I gives the co-latitude of the field line at the ionosphere, i.e., $\cos\theta_I = \sqrt{1 - R_I / L}$

- Note that in these coordinates, $u^3 = 0$ is at the equator, and $u^3 = \pm 1$ correspond to the ionospheres
- Coordinates singular at equator, so only good at mid-latitudes

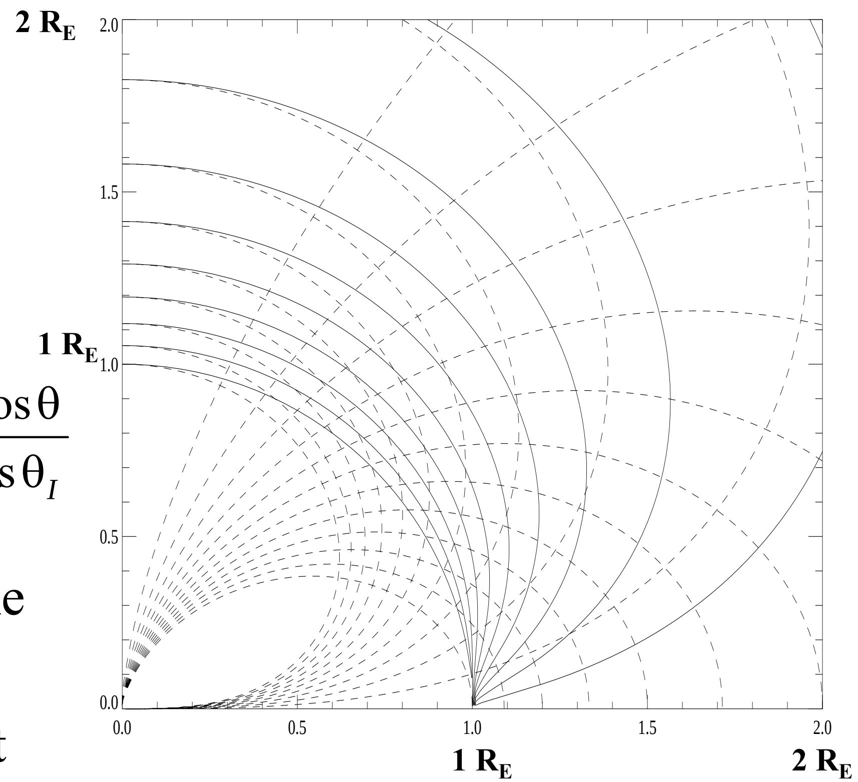

Contours of constant u^3 (solid) compared with coordinate lines for orthogonal system (dashed)

A short course in differential geometry
(D'haeseleer et al., 1991; Proehl et al., 2002)

- Two sets of basis vectors (not unit vectors):
  - Contravariant $\mathbf{e}^i = \nabla u^i$ (normal to surface u^i = constant)
  - Covariant $\mathbf{e}_i = \partial \mathbf{r} / \partial u^i$ (tangent to u^i coordinate curve)
  - Note that we have $\mathbf{e}^i \cdot \mathbf{e}_j = \delta^i_j$
  - For a vector **A**, we can write $A^i = \mathbf{A} \cdot \mathbf{e}^i$, $A_i = \mathbf{A} \cdot \mathbf{e}_i$
- Metric tensor: $g_{ij} = \mathbf{e}_i \cdot \mathbf{e}_j$
  - Gives length element: $ds^2 = g_{ij} du^i du^j$ (sum implied)
  - Scale factors $h_i = \sqrt{g_{ii}} = |\mathbf{e}_i|$
- Jacobian: $J = \mathbf{e}_1 \cdot (\mathbf{e}_2 \times \mathbf{e}_3) = \left[\mathbf{e}^1 \cdot (\mathbf{e}^2 \times \mathbf{e}^3) \right]^{-1} = \sqrt{\det g}$
  - Gives volume element: $dV = J du^1 du^2 du^3$
- Vector relations can be written in terms of these quantities, e.g.,

$$\nabla \times \mathbf{A} = \frac{1}{J} \varepsilon^{ijk} \frac{\partial A_k}{\partial u^j} \mathbf{e}_i$$

Contravariant and Covariant Basis Vectors

- $\mathbf{e}^1$ is perpendicular to field, e_3 is parallel.
- At ionosphere, $\mathbf{e}_1$ is horizontal and northward, $\mathbf{e}^3$ is radially inward.
- g_{13} is proportional to cosine of angle between $\mathbf{e}_1$ and $\mathbf{e}_3$
- g_{13} is biggest at ionosphere and near equator; angle becomes 90° at larger distances and near pole.

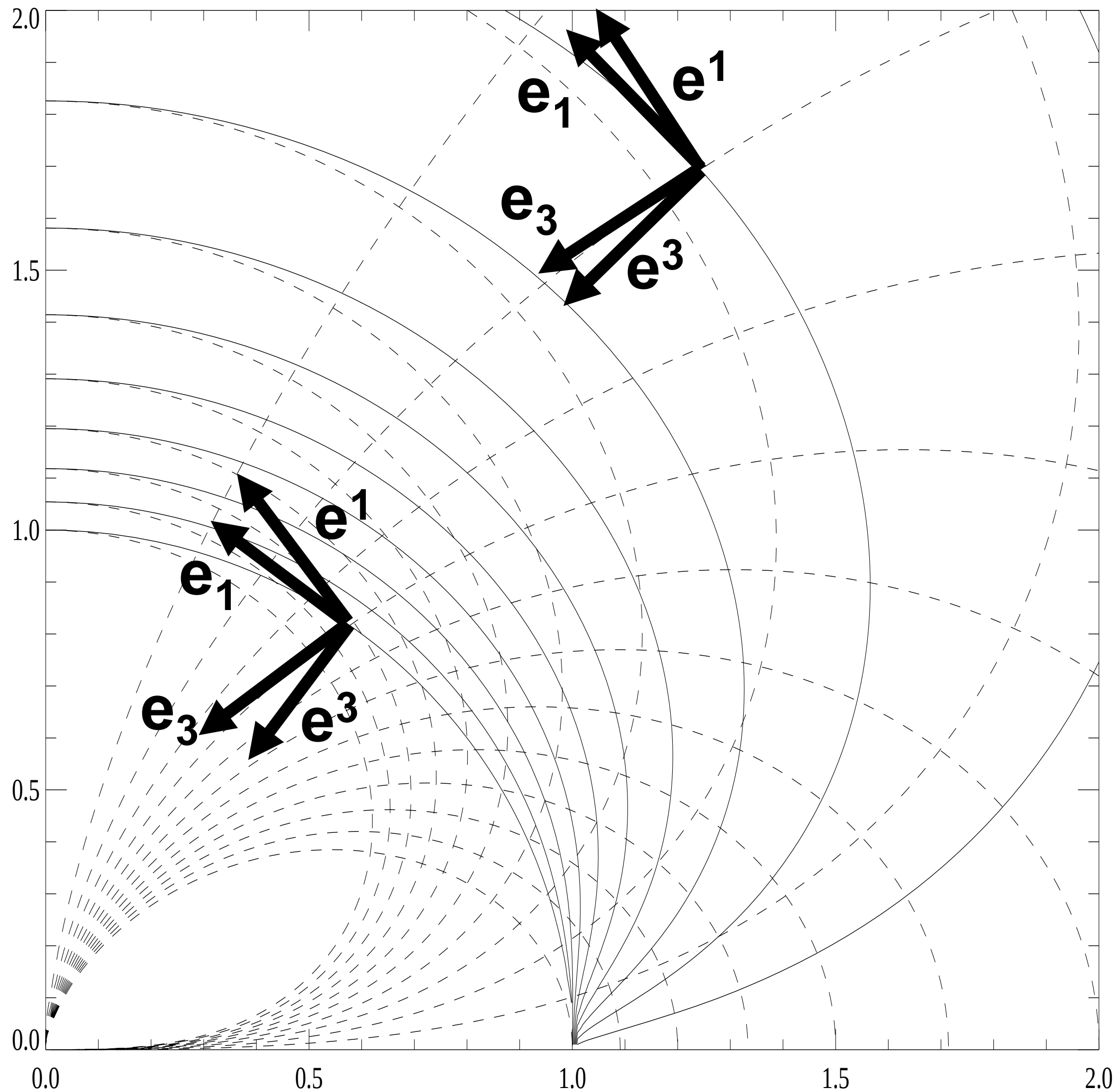

Wave equations in modified dipole coordinates: ideal MHD

- Wave equations can now be written as:

$$\frac{\partial E^1}{\partial t} = \frac{V^2}{J}\left(\partial_2 B_3 - \partial_3 B_2\right)$$

$$\frac{\partial E^2}{\partial t} = \frac{V^2}{J}\left(\partial_3 B_1 - \partial_1 B_3\right)$$

$$E_3 = 0$$

$$\frac{\partial B^1}{\partial t} = \frac{1}{J}\partial_3 E_2$$

$$\frac{\partial B^2}{\partial t} = -\frac{1}{J}\partial_3 E_1$$

$$\frac{\partial B^3}{\partial t} = -\frac{1}{J}\left(\partial_1 E_2 - \partial_2 E_1\right)$$

Note that E_1 and E_2 are constant along field lines in electrostatic case

- The fields are related by:

$$E^1 = g^{11} E_1 \quad \Rightarrow \quad E_1 = \frac{E^1}{g^{11}} \qquad E_2 = g_{22} E^2$$

$$B_1 = g_{11} B^1 + g_{13} B^3 \qquad B_2 = g_{22} B^2 \qquad B_3 = g_{31} B^1 + g_{33} B^3$$

- "Physical" fields as in dipole coordinates are (same for E)

$$B_\nu = h_\nu B^1 \qquad B_\varphi = h_\varphi B^2 = B_2 / h_\varphi \qquad B_\mu = B_3 / h_\mu$$

$$h_\nu = \frac{r^2}{R_I \sin\theta \sqrt{1 + 3\cos^2\theta}} \qquad h_\varphi = r\sin\theta \qquad h_\mu = \frac{r^3 \cos\theta_I}{R_I^2 \sqrt{1 + 3\cos^2\theta}}$$

Only new factor

Modeling Pi2 pulsations

Model is driven by a compressional pulse at midnight given by a damped oscillation at 50 seconds

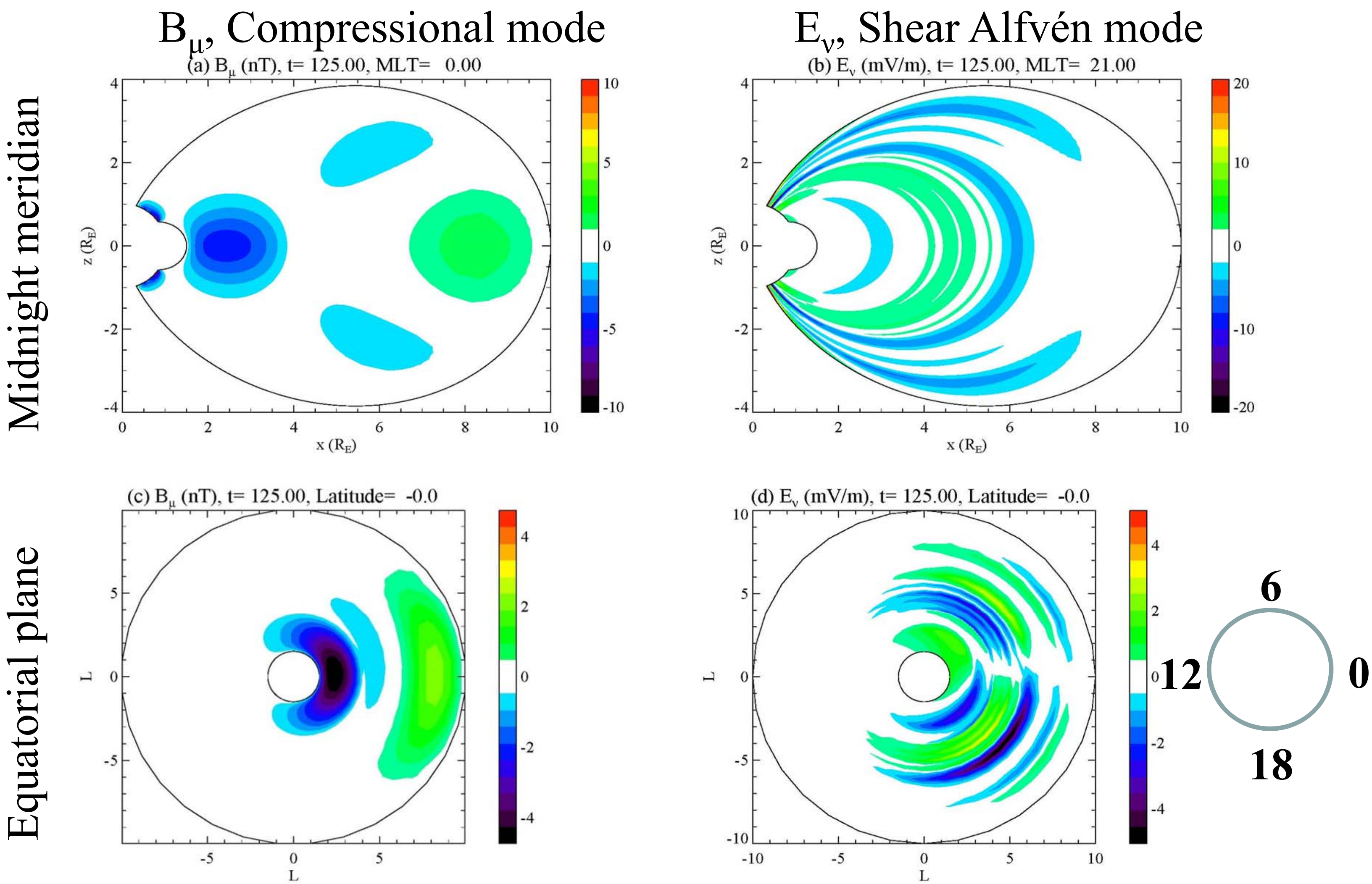

Results: B_μ and E_ν in meridian and equator

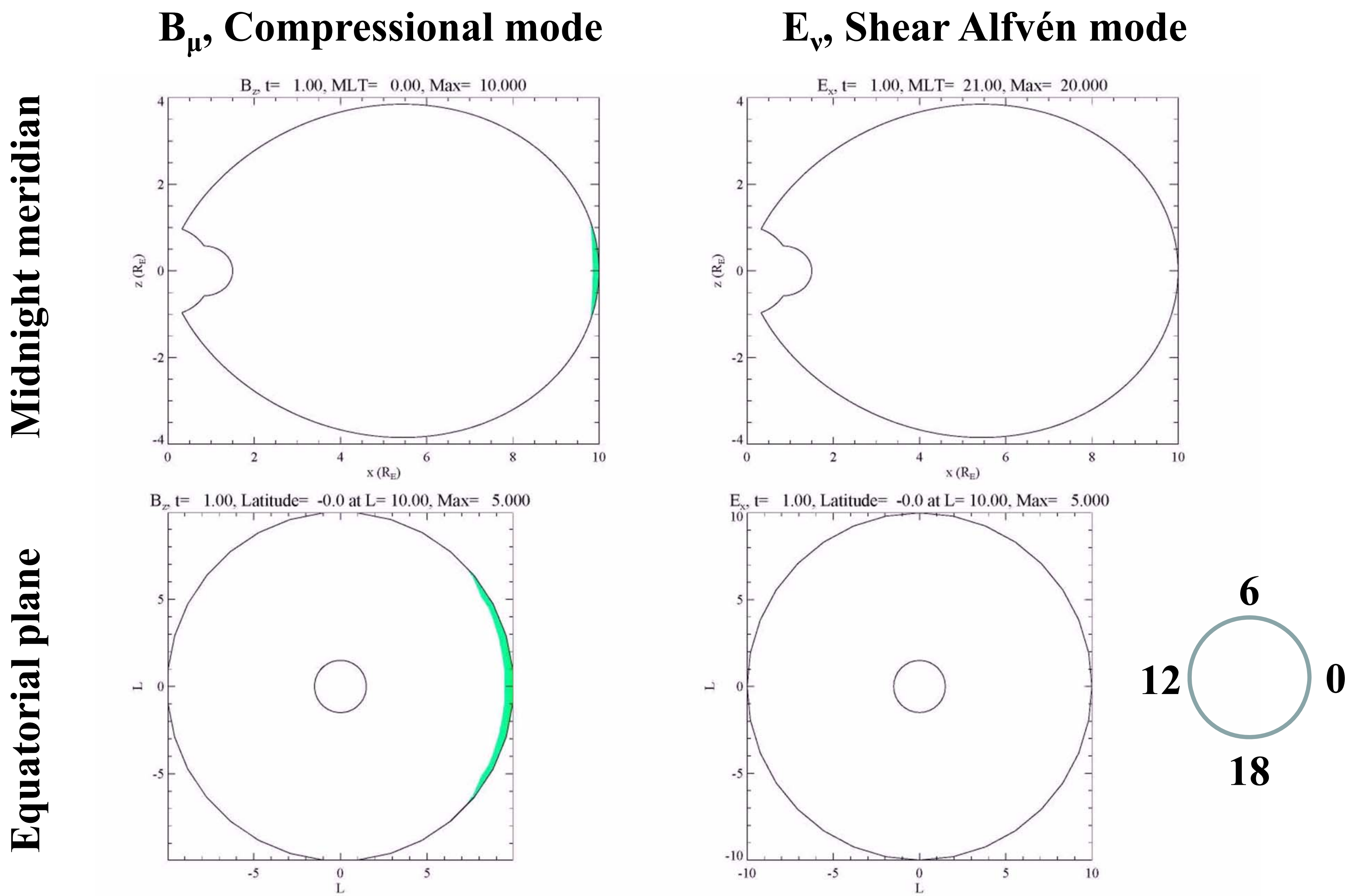

Comparison of B_μ and E_φ: Standing wave structure in plasmasphere

- Plot shows B_μ (solid) and E_φ (dashed) as function of time at midnight MLT
- 90 degree phase shift seen for L < 4 (in plasmasphere)

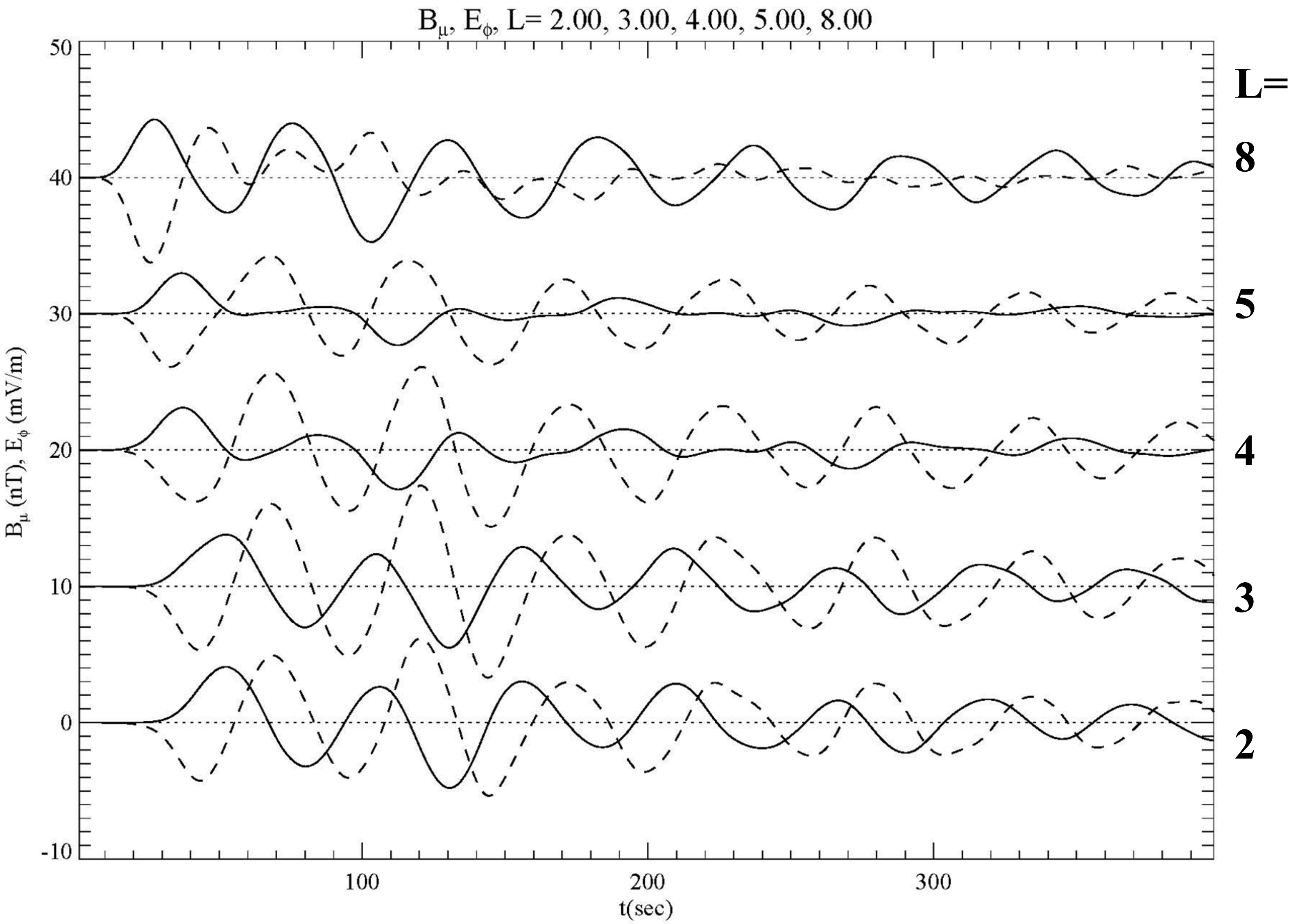

Example: Modeling of Pc4 pulsations

- Dai et al. (2013, 2015) studied poloidal Pc4 waves with Van Allen Probes
- Non-compressional (high *m*) poloidal waves observed in late storm recovery phase
- But high-*m* waves are cut off, cannot be externally driven
- Solution: Introduce fluctuating current source to model decaying ring current (McEachern, Ph.D. thesis, 2016)
- 2.5 dimensional model: azimuthal variation ~ $e^{im\varphi}$
- Waves largely trapped just outside the plasmapause

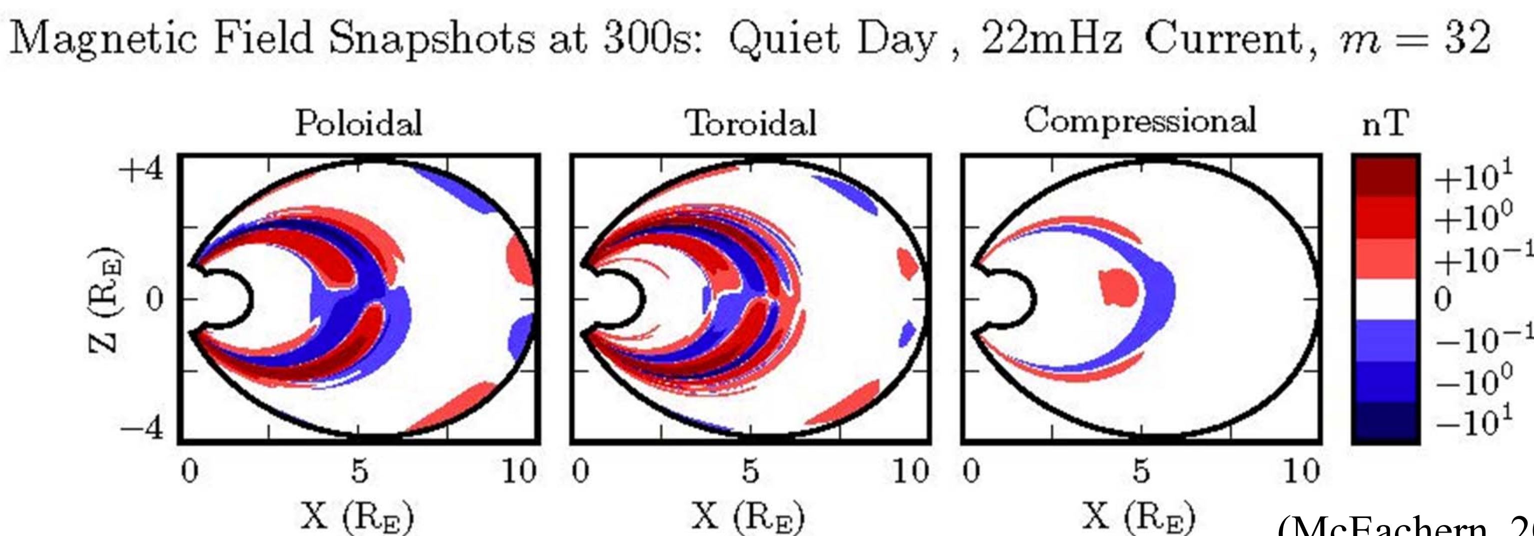

(McEachern, 2016)

Higher Frequency (Pc1, Pi1) ULF Waves: Dipole Model with full ionosphere

(Waters et al., 2013; Lysak et al., 2013)

- At higher frequencies ($f > 0.1$ Hz), need to consider ionospheric structure
- Hall conductivity couples shear Alfvén and fast modes
- Presence of fast mode implies ionospheric electric field not electrostatic
- Strong gradients of Alfvén speed above ionosphere become important: Ionospheric Alfvén Resonator
- New model includes distributed Pedersen, Hall and parallel conductivities and inductive ionosphere

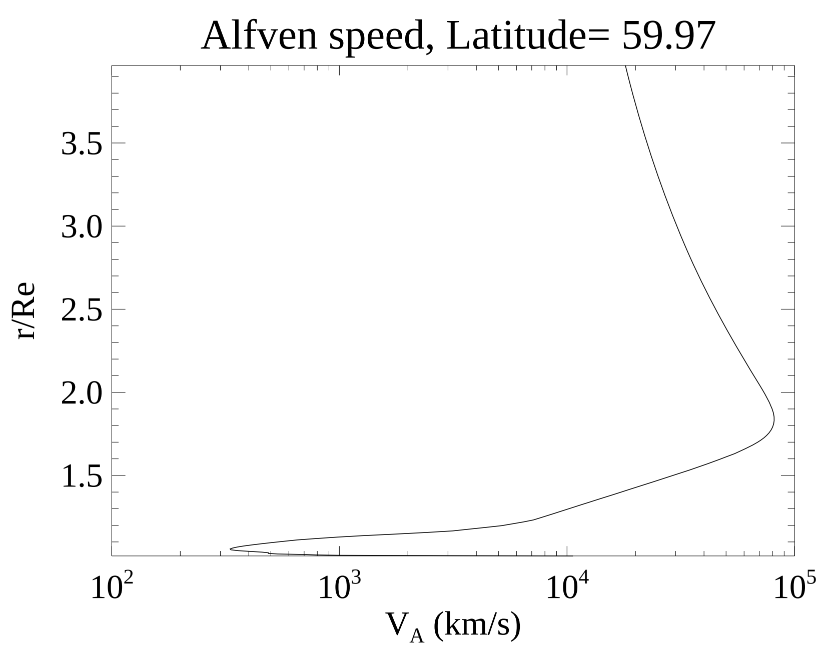

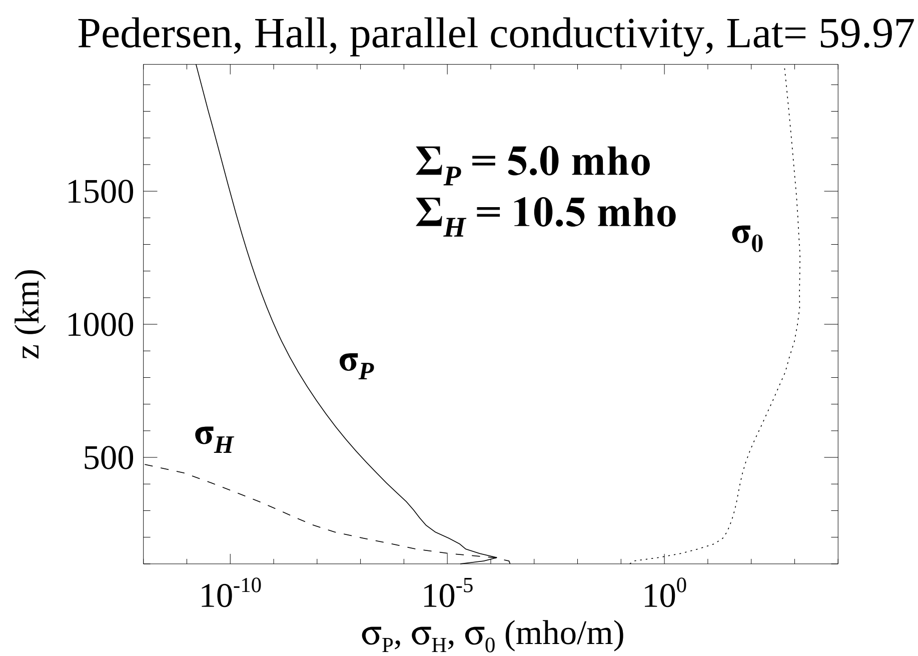

Wave equations with ionospheric conductivity

- With ionospheric conductivities, current is $\mathbf{j} = \sigma_P \left(\vec{\mathbf{1}} - \hat{\mathbf{b}}\hat{\mathbf{b}} \right) \cdot \mathbf{E} - \sigma_H \mathbf{E} \times \hat{\mathbf{b}} + \sigma_0 \hat{\mathbf{b}}\hat{\mathbf{b}} \cdot \mathbf{E}$
- Then the perpendicular components of Ampere's Law become

$$\varepsilon_\perp \frac{\partial \mathbf{E}_\perp}{\partial t} = \frac{1}{\mu_0} \left(\nabla \times \mathbf{B} \right)_\perp - \sigma_P \mathbf{E}_\perp + \sigma_H \mathbf{E}_\perp \times \hat{\mathbf{b}}$$

- Assuming a vertical magnetic field and using Cartesian components for simplicity we can write this as

$$\frac{\partial \mathbf{E}_\perp}{\partial t} + \frac{1}{\varepsilon_\perp} \begin{pmatrix} \sigma_P & -\sigma_H \\ \sigma_H & \sigma_P \end{pmatrix} \cdot \mathbf{E}_\perp = \frac{1}{\varepsilon_\perp \mu_0} \left(\nabla \times \mathbf{B} \right)_\perp \equiv \mathbf{F}_\perp$$

- Diagonalizing the matrix, we find eigenvalues $\lambda_\pm = (\sigma_P \pm i\sigma_H)/\varepsilon_\perp$
- Writing $E_\pm = E_x \pm iE_y$ and $F_\pm = F_x \pm iF_y$, ionospheric equations become $\left(\partial_t + \lambda_\pm \right) E_\pm = F_\pm$
- This can be directly integrated: $E_\pm(t + \delta t) = E_\pm(t) e^{-\lambda_\pm t} + \delta t F_\pm (t + \delta t/2) e^{-\lambda_\pm \delta t/2}$
- Note real part of $\lambda_\pm$ (σ_P) gives damping; imaginary part (σ_H) rotates electric vector in xy plane (Hughes rotation)
- These equations are written in terms of the full non-orthogonal components in the code..

Inductive Ionospheric Boundary Condition
(Yoshikawa and Itonaga, 1996; Lysak and Song, 2006)

- Many M-I coupling models use an electrostatic boundary condition and current conductivity to model the ionosphere: $j_{\|} = -\nabla \cdot \left(\overleftrightarrow{\boldsymbol{\Sigma}} \cdot \nabla \Phi \right)$
- However, this boundary condition only deals with the shear mode that carries field-aligned current; it does not provide a boundary condition for the fast mode waves.
- A more general boundary condition can be found by integrating Ampere's Law over the ionosphere:

$$\mu_0 \overleftrightarrow{\boldsymbol{\Sigma}} \cdot \mathbf{E} = \hat{\mathbf{r}} \times \Delta \mathbf{B}$$

- For vertical field lines and uniform $\overleftrightarrow{\boldsymbol{\Sigma}}$, taking the divergence yields the usual electrostatic condition, while taking the curl gives a second condition:

$$\Sigma_P \nabla_\perp \cdot \mathbf{E}_\perp - \Sigma_H \hat{\mathbf{r}} \cdot \left(\nabla \times \mathbf{E}_\perp \right) = -j_{\|}$$

$$\Sigma_H \nabla_\perp \cdot \mathbf{E}_\perp + \Sigma_P \hat{\mathbf{r}} \cdot \left(\nabla \times \mathbf{E}_\perp \right) = (1/\mu_0) \Delta \left(\partial B_r / \partial r \right)$$

- These equations illustrate the coupling of the shear mode (div E) and the fast mode (curl E) by the Hall conductivity.
- Note that this equation requires knowledge of **B** in the atmosphere.

The Atmospheric Solution

- Implementation of this model requires a solution below the ionosphere.
- Assume atmosphere is perfectly insulating, ground is perfectly conducting
- Then in atmosphere can use magnetic scalar potential

$$\nabla \cdot \mathbf{B} = 0,\ \nabla \times \mathbf{B} = 0 \ \Rightarrow \mathbf{B} = \nabla\Psi,\ \nabla^2\Psi = 0$$

- Field is “frozen-in” to ground, so $B_r = \partial\Psi / \partial r = 0$
- Radial magnetic field is continuous through layer, so Ψ is set by matching solution to simulation B_r
- Solution can be written in terms of spherical harmonics, modified to fit simulation boundaries:

$$\Psi(r,\theta,\varphi) = \sum_{l.m}\left(A_{lm} r^{\nu_l} + B_{lm} r^{-(\nu_l+1)}\right) y_{lm}(\theta,\varphi)$$

- Note that this solution allows direct calculation of ground magnetic fields as well as field just below ionosphere.

Ionospheric Shielding Effect

- Ionospheric Pedersen conductivity acts to shield higher frequency waves (collisional skin depth) $\delta = \sqrt{2/\mu_0 \omega \sigma_P}$
- Results are shown from a numerical model of Alfvén wave propagation including full ionosphere (Lysak et al., 2013)
- Model is driven with a broad-band “white noise” spectrum consisting of 100 waves from 0-2 Hz with equal amplitudes and random phases.
- It can be seen that the higher frequency components are attenuated at lower altitudes in the ionosphere

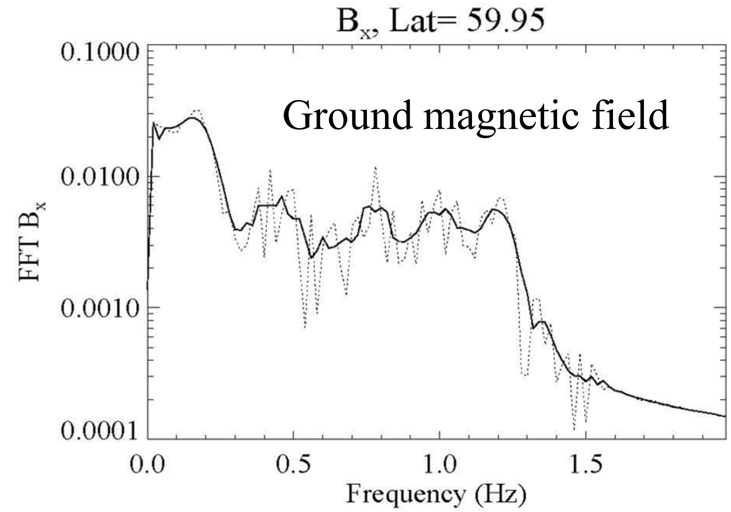

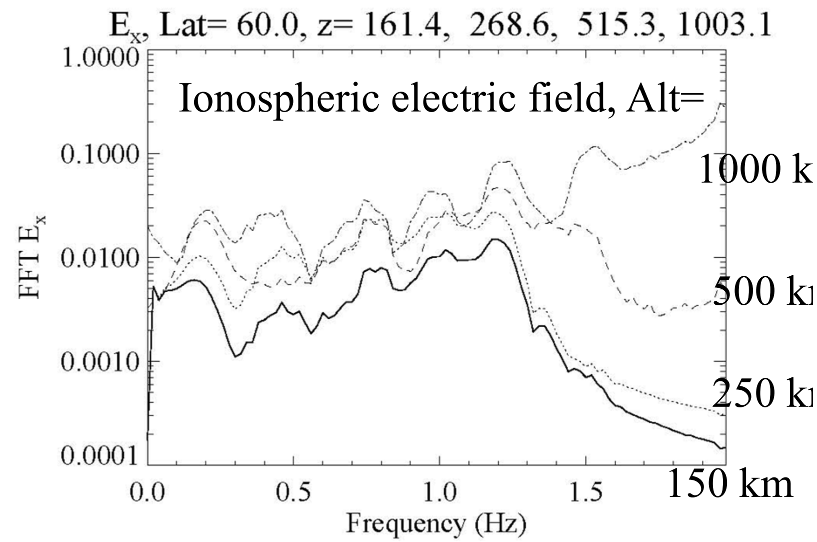

Ionospheric Alfvén Resonator

- Alfvén speed rises sharply above ionosphere due to exponential fall of plasma density.
- Wave propagation speed goes back to the speed of light at altitudes below the ionosphere.
- The minimum in Alfvén speed in ionosphere forms a resonant cavity for shear Alfvén waves (Ionospheric Alfvén Resonator) and a waveguide for fast mode waves in 1-10 s period range.
- Fast and shear Alfvén modes are coupled by the Hall conductivity in the ionosphere.

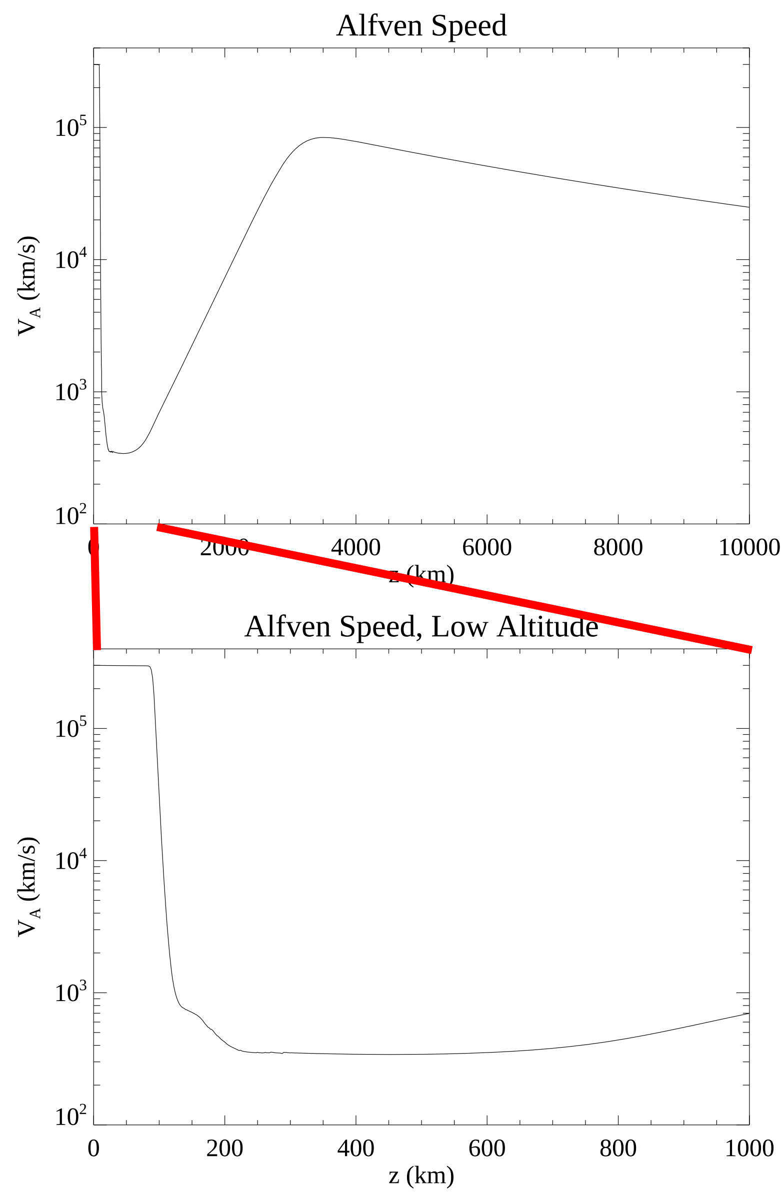

IAR Mode Structures: First 3 Harmonics, m=0

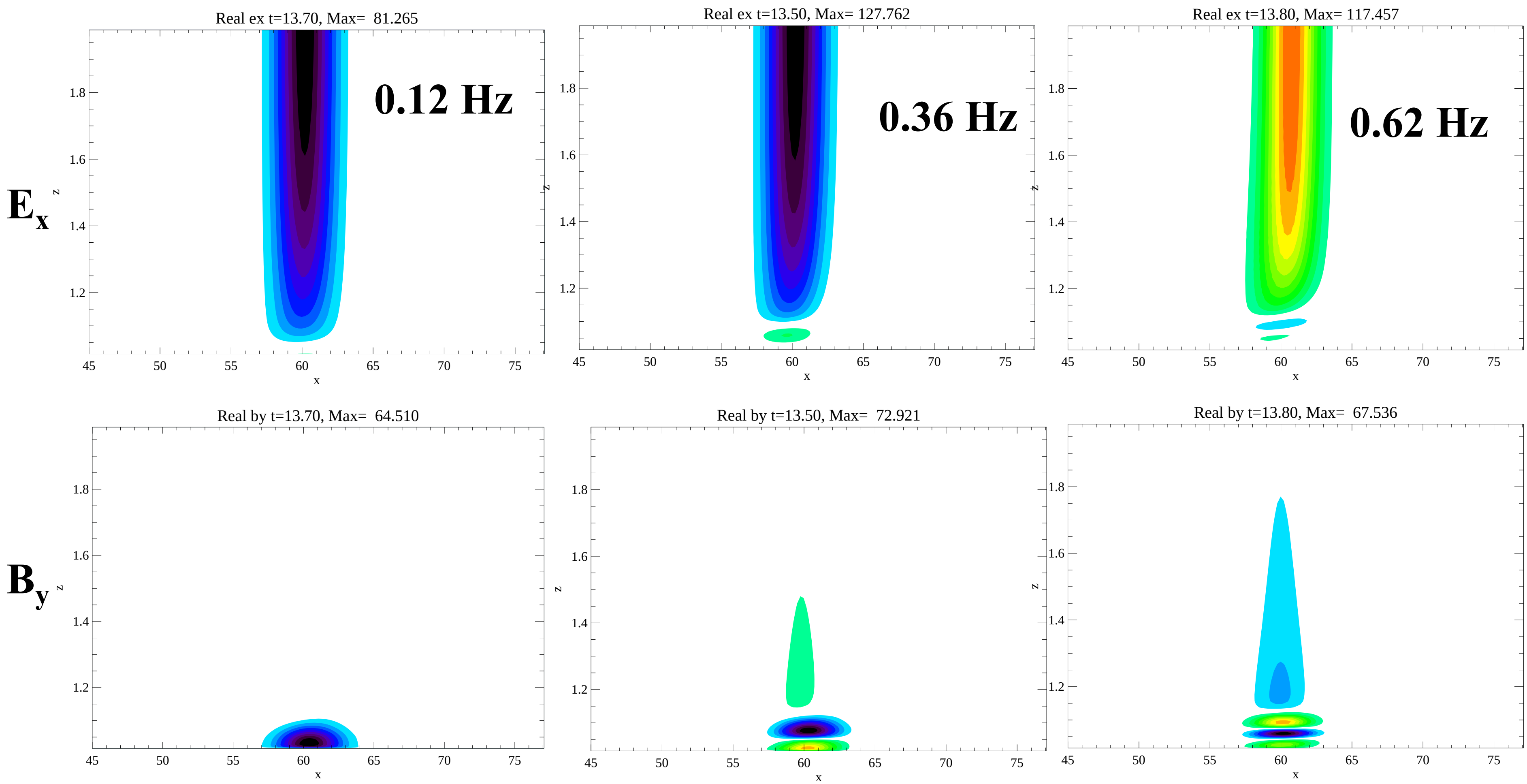

- E_x (top) and B_y (bottom) mode structures for 0.12, 0.36, and 0.62 Hz runs showing harmonic structures in IAR. Only region below 2 R_E is shown

Mode Coupling: Effect of Hall conductivity

- Hall currents couple shear mode and fast mode: Fast mode propagates horizontally in Pc1 waveguide (e.g., Fraser, 1976; Engebretson et al., 2002)
- This propagation gives characteristic pattern of polarization, reproduced in simulations of Woodroffe and Lysak (2012):

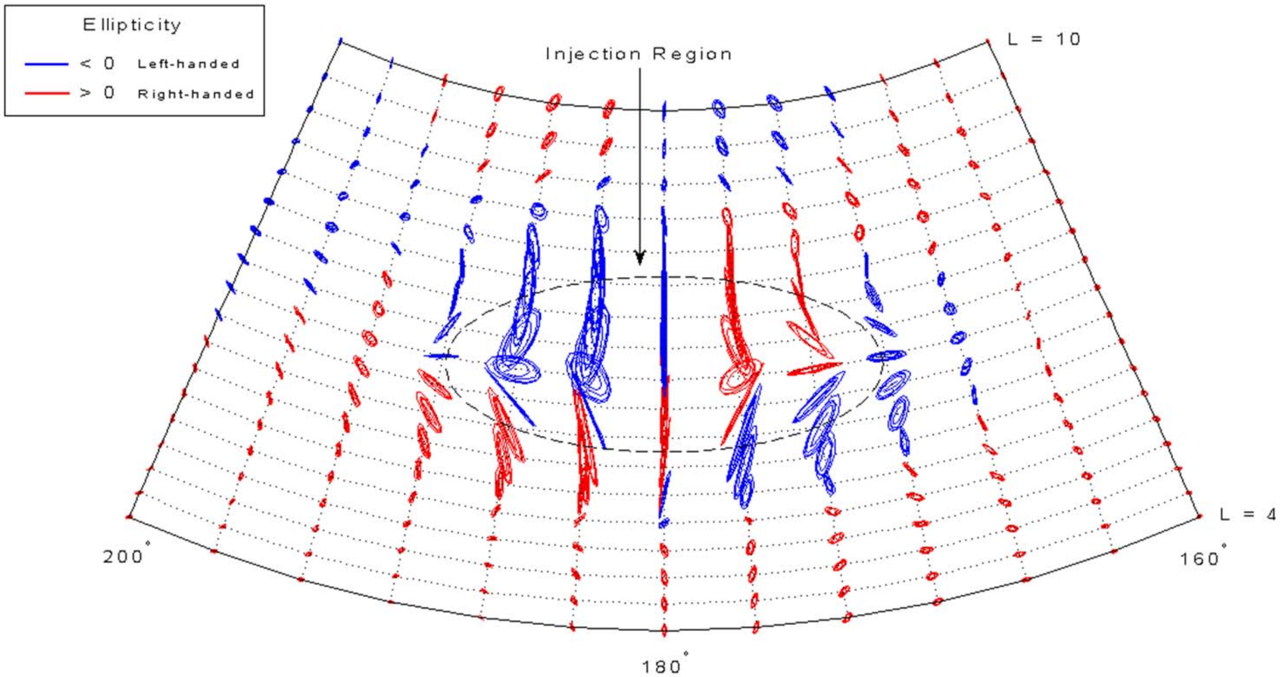

Pc1 “Pearls”

- Pc1 waves often occur in wave packets, called “pearls” (e.g., Fraser, 2006)

- System driven by a 10-second long wave packet with given frequency
- IAR resonant frequency is 1.22 Hz in this case
- Ground B_x (poleward) component shown (left), with Poynting flux (right)
- Off-resonant frequency (0.96 Hz) dies out quickly; higher frequency (2 Hz) doesn’t penetrate ionosphere
- Resonant wave (1.22 Hz) gives longer lasting wave train due to multiple reflections.

Ground B_x | Parallel Poynting flux

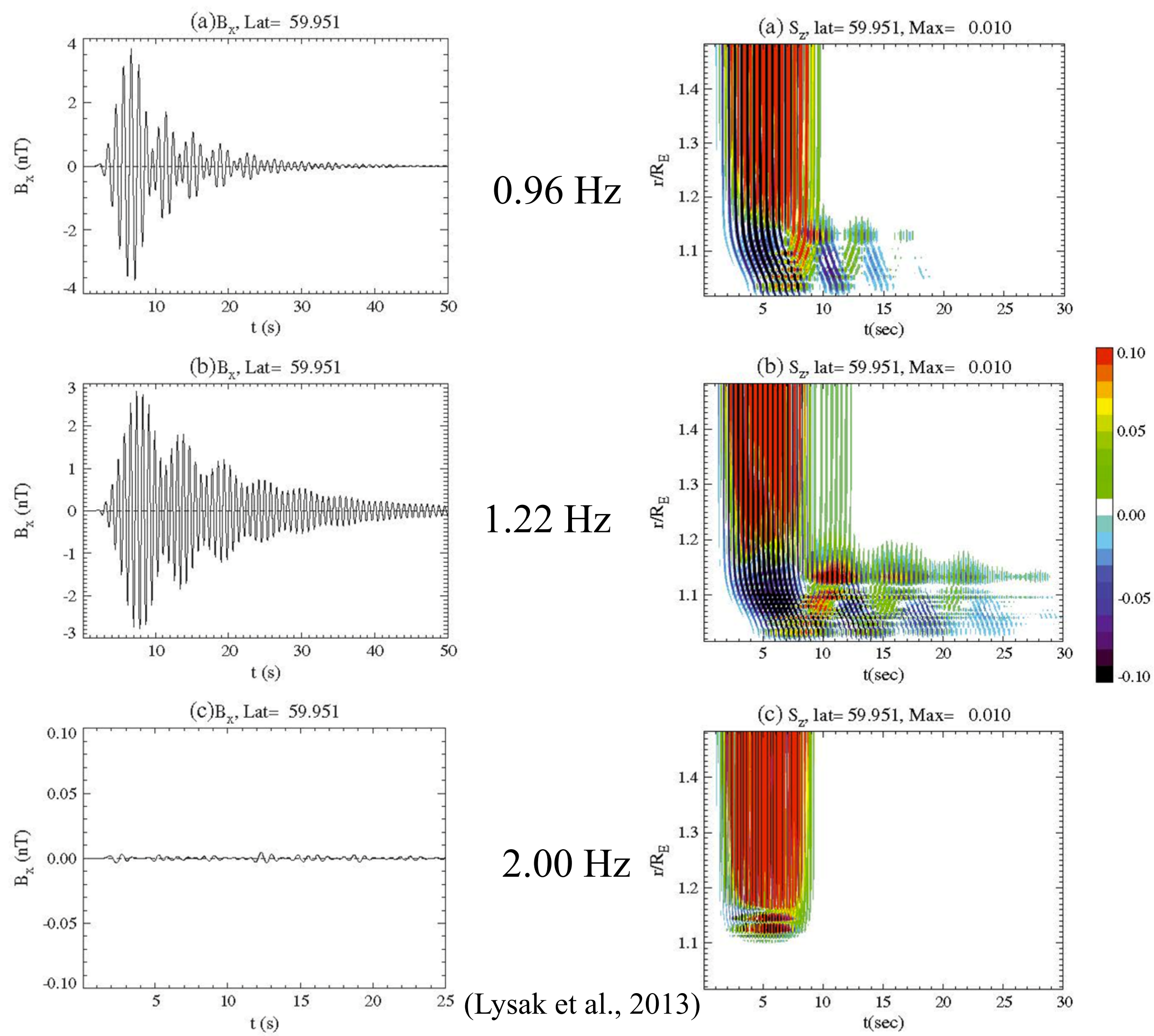

(Lysak et al., 2013)

3d ULF Wave Model

- Fully 3-d wave model needed to avoid assumption of single *m* number
- Height-resolved ionospheric model gives more realistic ionospheric fields.
- Ground magnetic fields calculated from spherical harmonic expansion.
- Region from L = 1.5 to L = 10 modeled. Plasmapause at L=4.
- Model is 3d, with 128x64x318 cells in L-shell (ν), MLT (φ), and distance along field line (μ), using staggered Yee grid
- Compressional driver on outer boundary, Gaussian in latitude and longitude. Inner L-shell uses $B_\mu = 0$ boundary condition (no compression).
- Newest feature: Ionospheric conductivity based on solar zenith angle; subsolar point can be varied for seasonal differences.

Density and Alfvén speed profiles

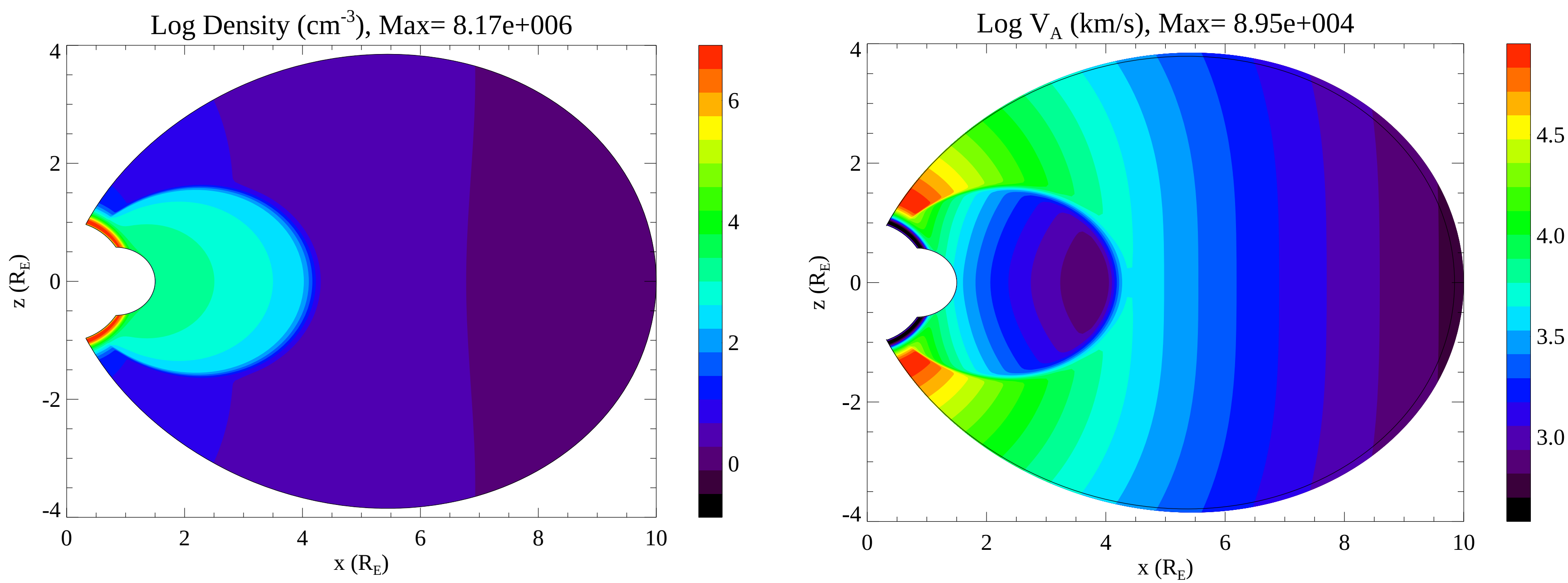

- Model based on ionospheric model as in Kelley (1989), plasmasphere model of Chappell (1972), 1/*r* density dependence along high-latitude field lines.
- Plasmapause at L=4, width of transition 0.1 R_E

Alfvén travel time profile

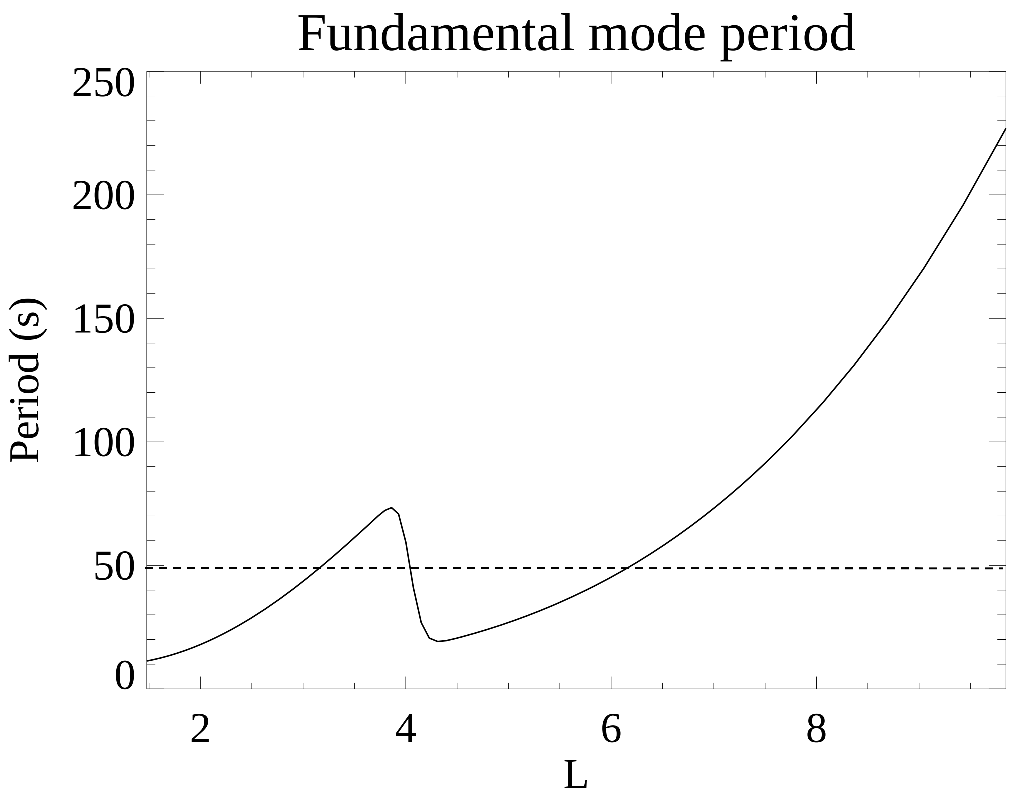

- 50 sec driver resonates near L = 3 and 6, consistent with simulation results
- Third harmonic (150 sec) at L = 8.5
- Note range of frequencies at plasmapause: excitation of plasmapause surface wave?

Day/Night Conductivity Effects

- Sun is placed at equator: equinox conditions
- Ionosphere varies from daytime profile to nighttime profile based on solar zenith angle:

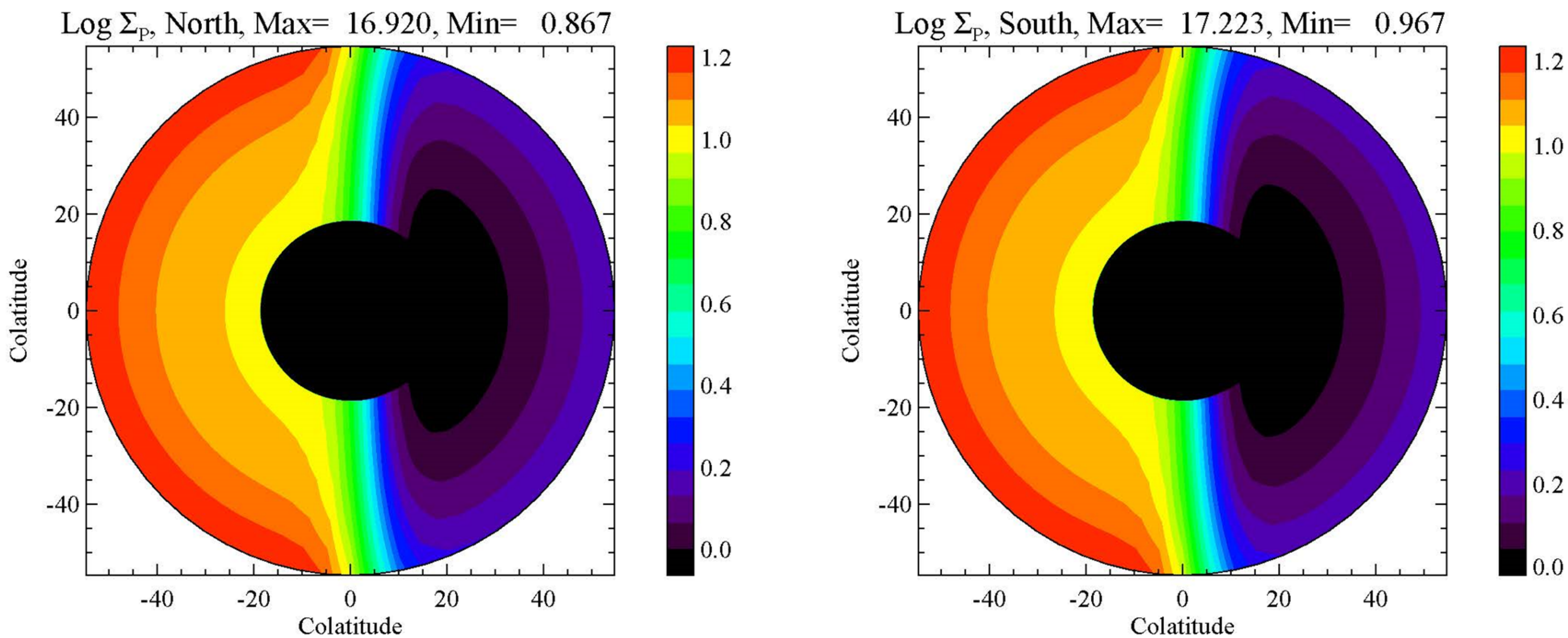

Toroidal Fields: Dayside Driving

- Waves driven by compression at noon, 50 second period
- Field magnitudes scaled to ionospheric altitude

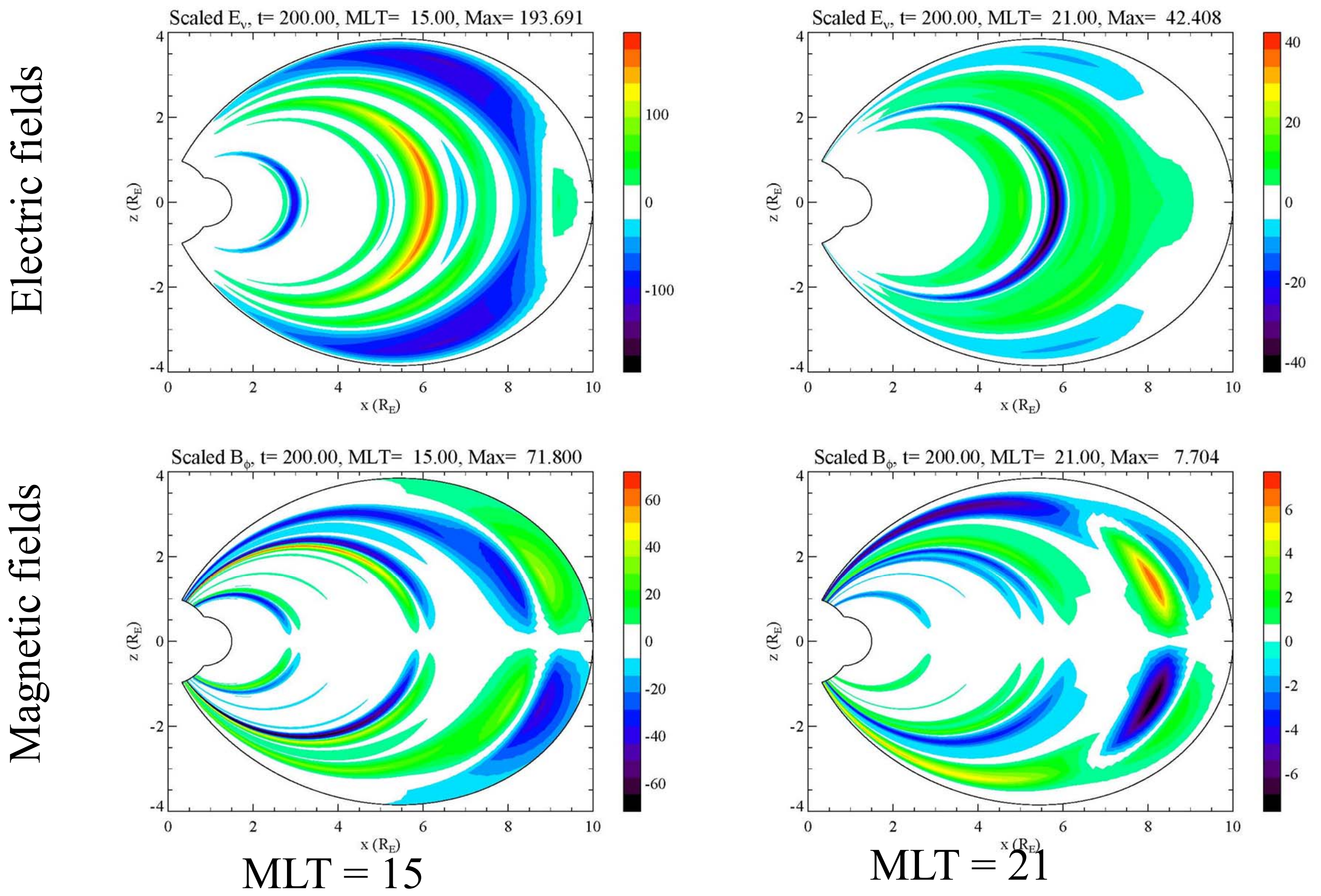

Day-night differences: Nightside driving

- Waves driven by compression at midnight, 50 second period
- Dayside fields stronger than nightside fields for dayside driving

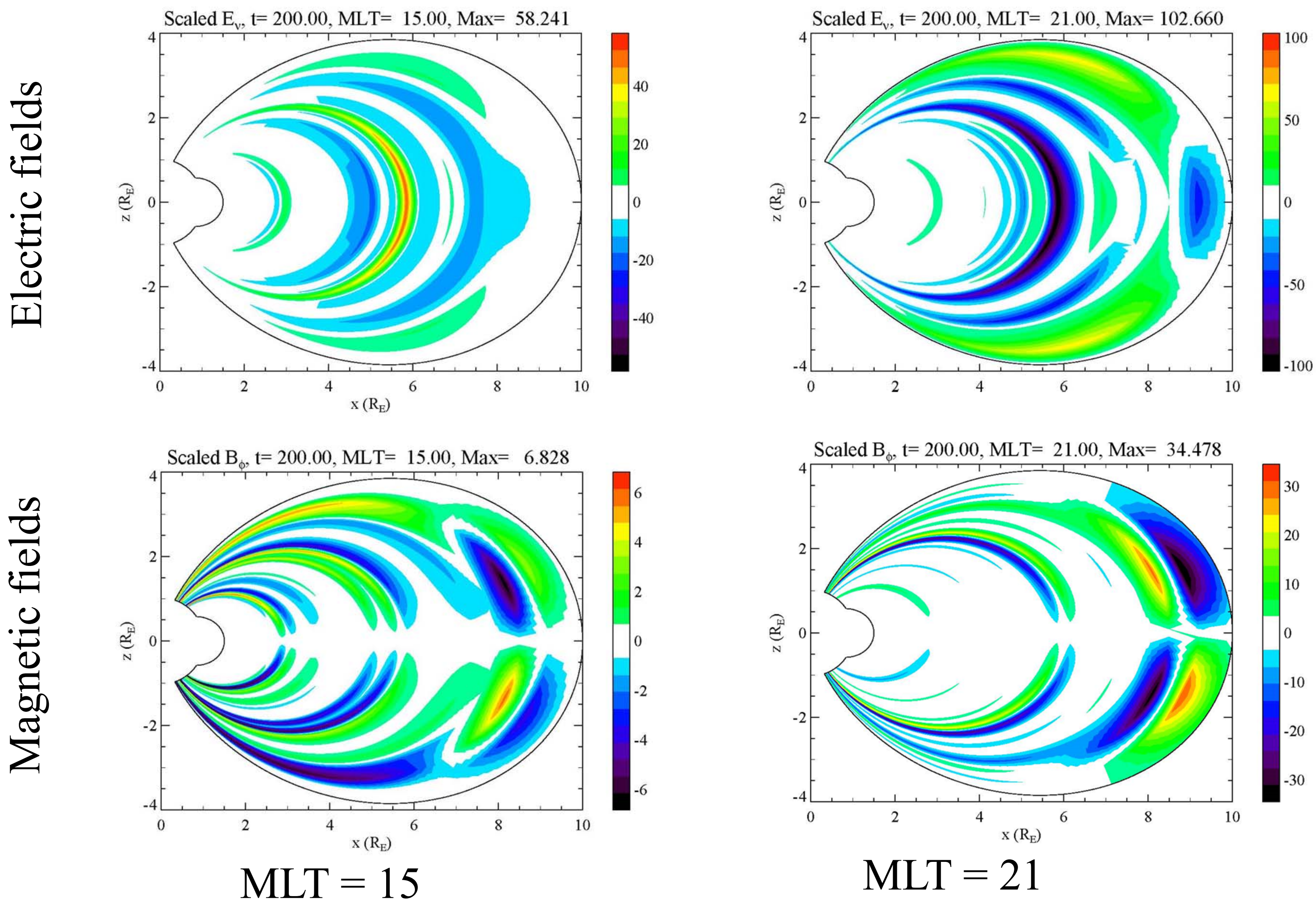

Ground magnetic fields

- For dayside driving, ground magnetic fields stay on dayside, but for nightside driving, field line resonances appear on dayside.
- Note dawn-dusk asymmetry: results from Hall conductivity

Noon

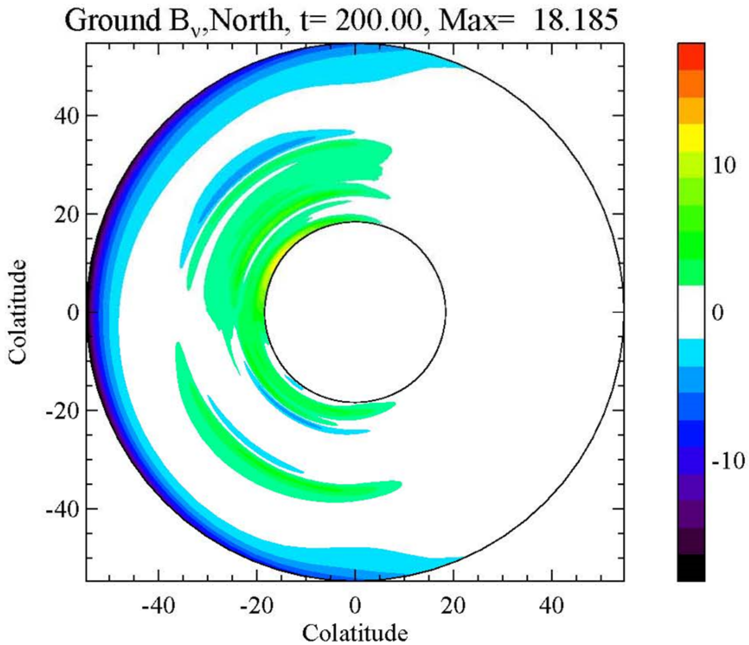

Dayside Driving

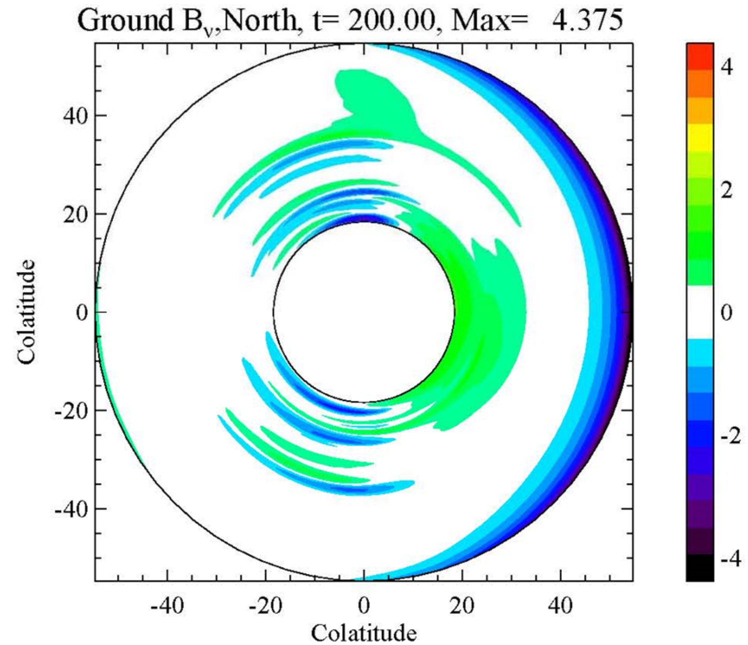

Nightside Driving

Northern Summer: Search for ¼ waves

- At solstice, one end of field line can be in darkness while the other is sunlit
- In sunlit (high conductivity) hemisphere, electric fields are weak
- This can give rise to waves with node in one hemisphere and antinode in the other ("quarter waves": Obana et al., 2015)
- Conductivity models based on solar zenith angle at footpoint of field line, with Sun at 23° from equator

Σ_P, North

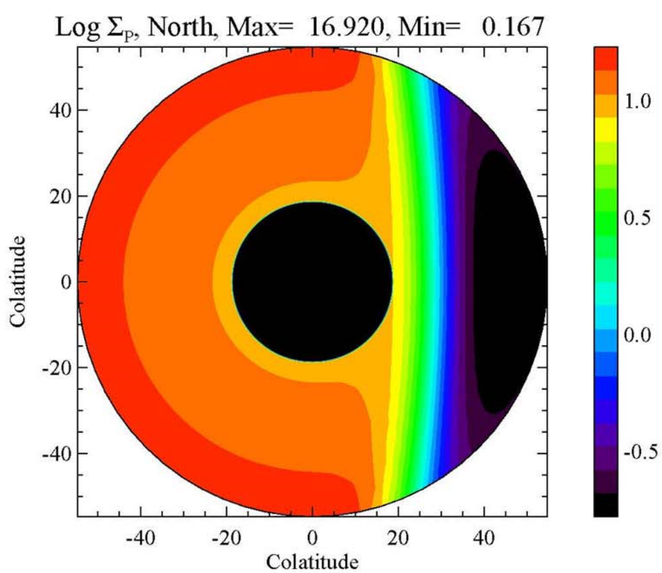

Σ_P, South

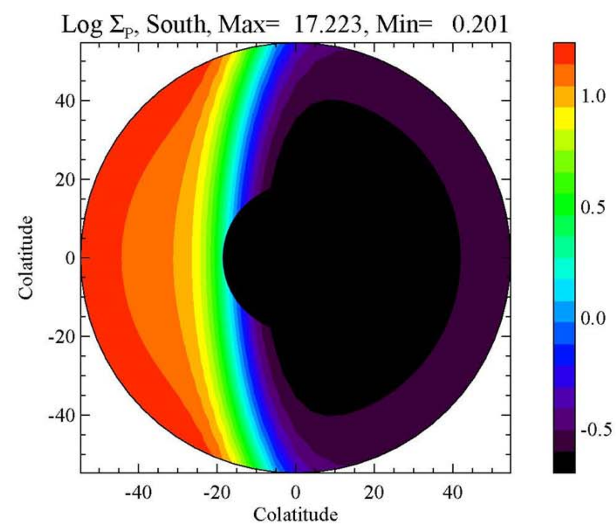

Northern Summer: Search for ¼ waves

- System driven at 100 second period on dayside
- Fields shown at dawn terminator (MLT = 6)
- Electric fields stronger in winter hemisphere, magnetic field in summer
- Poynting flux directed toward winter hemisphere (agrees with statistical results of Junginger et al., 1985)
- In contrast to symmetric case, field-aligned current flows from one hemisphere to the other (contours of B_φ approximate current flow lines)

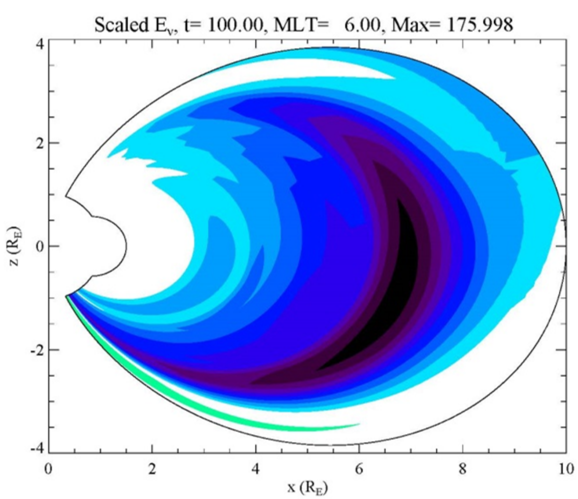

Electric field E_ν

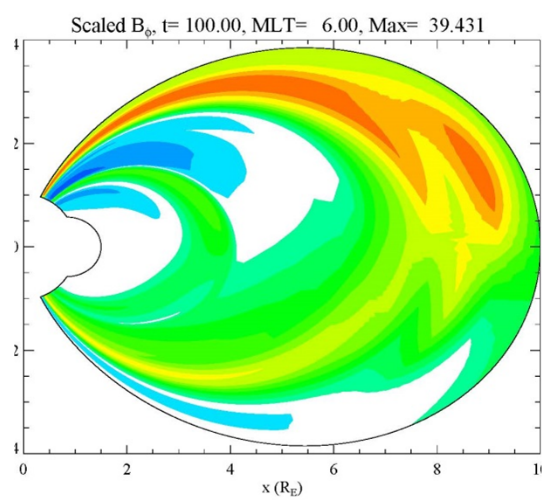

Magnetic field B_φ

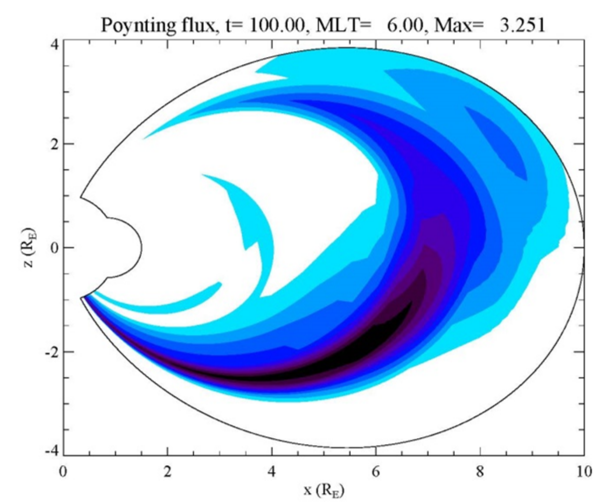

Field-aligned Poynting flux (blue southward)

Electric and Magnetic Fields at 6 MLT

Northern summer conditions at dawn terminator

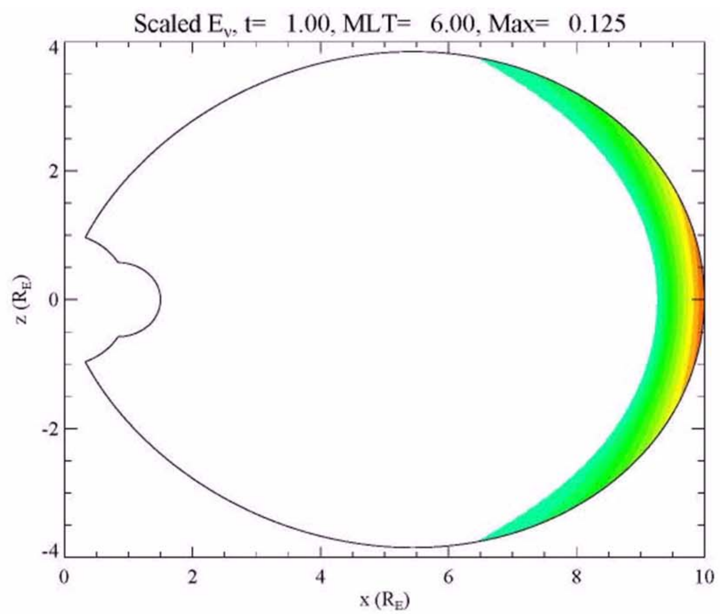

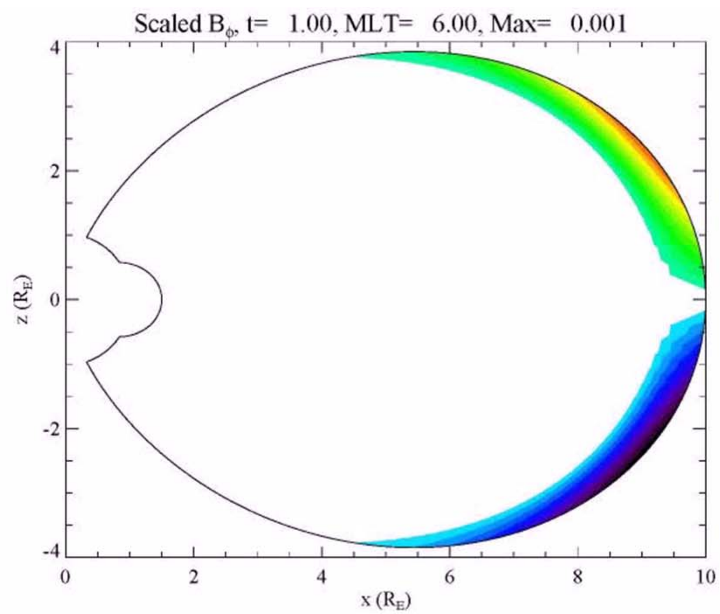

Poynting Flux at 6 MLT

Northern summer conditions at dawn terminator

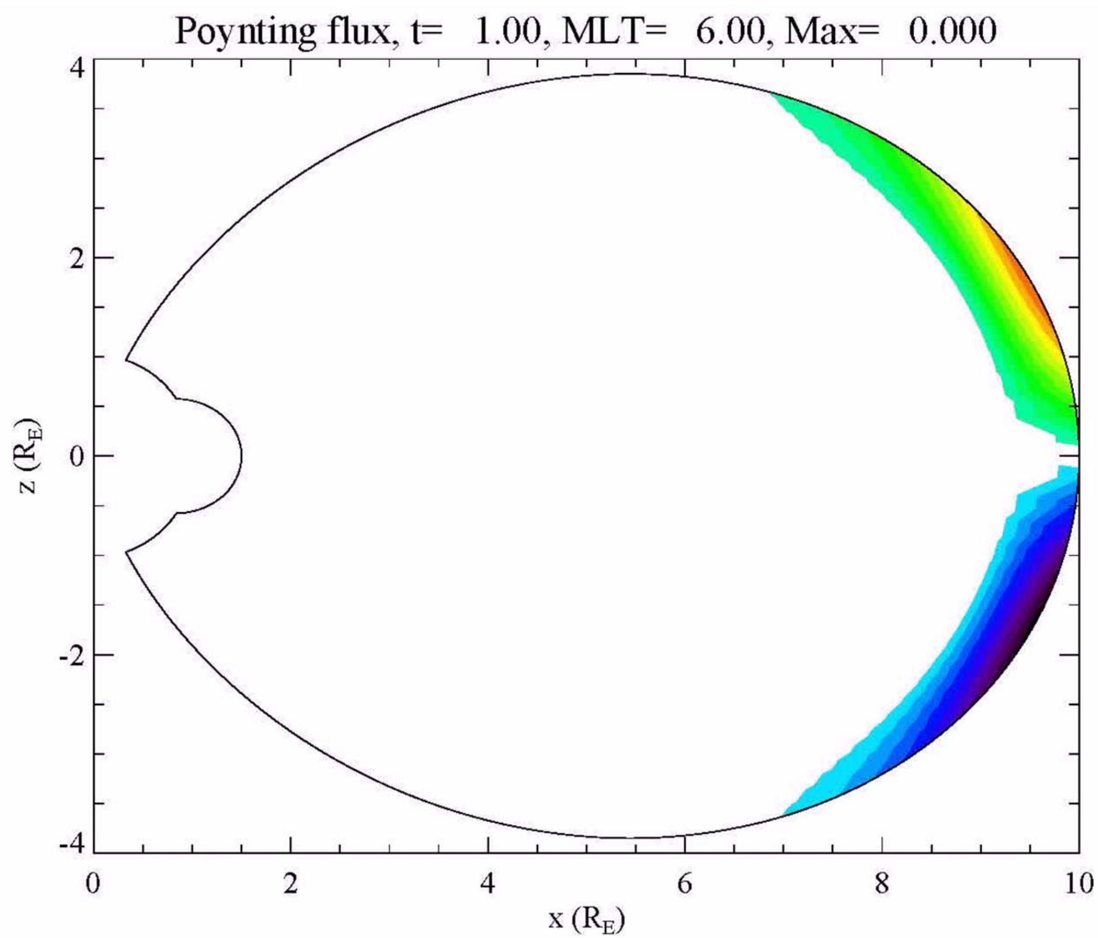

Things not covered

- Simple static conductivity model is not always valid
  - Ionospheric feedback: self-consistent precipitation can change conductivity (e.g., Lysak and Song, 2002; Streltsov and Lotko, 2008)
  - Would be preferable to include full ionospheric and thermospheric dynamics (e.g., Otto et al., 2003; Sydorenko and Rankin, 2012)
    - However, collision frequency high enough so inertial terms higher-order correction.
- Kinetic Alfvén waves: a whole separate talk
  - Electron inertia gives broad-band electron acceleration at low altitudes (e.g., Lysak and Song, 2008)
  - In warmer plasma region, electron pressure can lead to parallel electric fields (e.g., Lysak and Song, 2011)
  - Hybrid models with particle electrons can better describe electron acceleration including effects of electron trapping (e.g., Watt and Rankin, 2010; Damiano and Johnson, 2012)